This article has been accepted for publication in IEEE Journal on Selected Areas in Communications. This is the author's version which has not been fully edited and content may change prior to final publication. Citation information: DOI 10.1109/JSAC.2024.3459079

Dual-Functional UAV-Empowered Space-Air-Ground Networks: Joint Communication and Sensing

Xiangdong Zheng, Yuxin Wu, Lisheng Fan, Xianfu Lei,
Rose Qingyang Hu, *Fellow, IEEE*, and George K. Karagiannidis, *Fellow, IEEE*

***Abstract*—In this paper, we investigate a sensing-enabled integrated space-air-ground (SAG) data collection network, in which an unmanned aerial vehicle (UAV) can not only work singly to sense data from multiple targets but also collaborate with a low-earth orbit (LEO) satellite to collect communication data from multiple users. Since the coverage of the UAV is much smaller than that of the LEO satellite, we first determine the set of usable users and targets for the UAV by analyzing the signal-to-noise ratios between the UAV and the users and targets. Based on this, we pose an optimization problem designed to maximize the total amount of data collected in the network while satisfying the constraints of UAV energy consumption, memory capacity, and minimum amount of sensor data per target. Moreover, considering that the network consists of three layers and the UAV has dual functions of communication and sensing, this problem is solved by jointly optimizing the scheduling of the users' data upload scheme, the UAV trajectory, and the allocation of communication and sensing time. However, the formulated problem is a mixed integer nonlinear programming (MINLP) problem, so it is difficult to find the optimal solution. Therefore, we further design an alternating iterative optimization algorithm (AIOA) framework to find an appropriate solution. Specifically, we alternately optimize the UAV trajectory, time allocation strategy, and data upload schedule in each iteration. Finally, simulation experiments validate the effectiveness of the AIOA and its superiority over other benchmarks in terms of the amount of data collected.**

***Index Terms*—SAG network, UAV trajectory optimization, data collection, communication and sensing.**

I. Introduction

As society accelerates its transformation to digitalization and intelligence, sixth-generation (6G) technology is developing rapidly. 6G can provide ultra-high speed, low-latency, and high-reliability communications to meet the requirements of future 6G applications [1], [2]. Meanwhile, 6G technology is also facilitating the development of Internet of Things (IoT) networks, leading to numerous IoT applications such as smart environmental monitoring, efficient energy management, and precision agriculture technologies [3]–[6]. However, most 6G-enabled IoT applications rely heavily on efficient and reliable data collection and processing capabilities, making data collection and analysis particularly critical. Although 6G networks can offer unprecedented communication capabilities, this challenge still exists in remote and topographically complex areas. To meet this requirement, an integrated Space-Air-Ground (SAG) network has been proposed as a promising solution for data collection, with the unique advantage of being able to integrate satellite and airborne platform systems [7]–[9]. In particular, in remote areas that are difficult to cover with traditional communication technologies, the SAG network shows great potential [10].

Specifically, the integrated SAG network includes satellites, airborne platforms and ground nodes, with satellites and airborne platforms playing a central role in the SAG network structure. On the one hand, satellite communications are provided by geostationary orbit (GEO), medium earth orbit (MEO) and low earth orbit (LEO) satellites, each of which has its own specific service characteristics and application scenarios [11], [12]. In particular, GEO satellites are mainly used for broadcasting and weather monitoring, and MEO satellites are suitable for navigation services. LEO satellites are particularly suitable for the realization of SAG networks due to their low latency and high speed data transmission caused by their low orbits [13]–[15]. In this field, The StarLink project, recently built by SpaceX, has been proposed to build a constellation of a large number of small satellites in LEO to provide high-speed broadband Internet services to users around the world. In addition, the authors in [16] investigated downlink transmission strategies for large-scale multiple-input multiple-output (MIMO) LEO satellite communications systems. In addition, the authors in [17] investigated the reliable performance of downlink LEO satellite communication systems and also investigated UAV-based cooperative transmission to compensate for the large path loss caused by long transmission distances.

While LEO satellites provide extensive coverage for global connectivity, they still have limitations, such as high latency compared to terrestrial communications. In response, UAVs are being used as carriers for information acquisition, transmission and processing, complementing and extending LEO satellite communications. Taking advantage of UAV characteristics such as lower latency, high mobility, rapid deployment,

X. Zheng, Y. Wu, and L. Fan are with the School of Computer Science and Cyber Engineering, Guangzhou University, Guangzhou 510006, China (e-mail: xdzheng@e.gzhu.edu.cn; 2112106230@e.gzhu.edu.cn; lsfan@gzhu.edu.cn).

X. Lei is with the School of Information Science and Technology, Institute of Mobile Communications, Southwest Jiaotong University, Chengdu 610031, China (e-mail: xflei@home.swjtu.edu.cn).

Rose Qingyang Hu is with the Department of Electrical and Computer Engineering, Utah State University, Logan, UT 84322 USA (e-mail: rosehu@ieee.org).

G. K. Karagiannidis is with Aristotle University of Thessaloniki, Greece and is also with Cyber Security Systems and Applied AI Research Center, Lebanese American University (AUL), Lebanon (e-mail: geokarag@auth.gr).

This work was supported in part by the NSFC (Nos. U23A20273/62271158).

The corresponding author of this paper is L. Fan.

Authorized licensed use limited to: Aristotle University of Thessaloniki. Downloaded on September 23,2024 at 10:14:54 UTC from IEEE Xplore. Restrictions apply.
© 2024 IEEE. Personal use is permitted, but republication/redistribution requires IEEE permission. See https://www.ieee.org/publications/rights/index.html for more information.

This article has been accepted for publication in IEEE Journal on Selected Areas in Communications. This is the author's version which has not been fully edited and content may change prior to final publication. Citation information: DOI 10.1109/JSAC.2024.3459079

and line-of-sight (LoS) channels, UAVs can serve as relays to effectively overcome the limitations of LEO satellites and improve the overall performance of the SAG network. In particular, UAVs can be rapidly deployed in targeted areas to provide various transmission services, such as point-to-point and wide-area data transmission services. When providing services, UAVs can operate in two communication modes: "hovering communication" and "flying communication", depending on whether the UAV is hovering or flying when providing services. Although UAVs have such advantages and benefit the SAG network, their limited battery capacity and high energy consumption should be considered to provide more sustainable services. To this end, the tradeoff between UAV energy consumption and information throughput has been extensively studied in the literature, such as [18], [19]. For example, the researchers in [19] aimed to minimize the total energy consumption of the UAV while satisfying the communication throughput requirements of the ground nodes. Therefore, they formulated and addressed an optimization problem involving complex considerations of UAV trajectory, communication time allocation, and mission completion time.

In the recent vision of wireless communications, 6G will not only provide ultra-high-speed, low-latency, high-reliability communication services, but also extend to high-precision sensing services [20]. However, as an important component of 6G, the SAG network has seen less research in the area of sensing, although there have been some studies exploring the use of UAVs in sensing missions [21]–[23]. In particular, a base station with dual-function radar communication (DFRC) capability can not only provide communication services, but also sense the environment, e.g. by collecting information on the target's position, speed, and shape, as well as information on human posture from radar echoes [20], [24]. However, due to limited resources, how to design DFRC schemes to balance communication and sensing performance is still a challenge. In this area, the UAV was designed to alternately transmit communication signals and sensing signals to achieve DFRC [25], [26]. In addition, the base station could transmit communication and sensing signals simultaneously to realize DFRC [27], [28]. In addition, a dual-function beamforming matrix of communication and sensing was designed to achieve DFRC [29]. Although the difference exists in the implementation of the aforementioned DFRC methods, the common goal of those is to optimize the efficiency of communication while ensuring the quality of sensing. Motivated by this, we consider a novel integrated SAG network, where the UAV can provide both communication and sensing services during flight.

In this paper, we study a sensing-enabled integrated SAG data collection network, where the UAV can not only work singly to sense data from multiple targets but also collaborate with the LEO satellite to collect communication data from multiple users. By taking into account that the service coverage of the UAV is much smaller than that of the LEO satellite, we first determine the set of serviceable users and targets for the UAV based on the signal-to-noise ratios (SNRs) between the UAV and users and targets. From this, we pose an optimization problem designed to maximize the total amount of data collected in the network, while simultaneously meet the constraints of the UAV energy consumption, memory capacity, and minimum amount of sensing data per target. Moreover, considering that the network encompasses three layers and the UAV has dual functions of communication and sensing, this problem can be solved by jointly optimizing the scheduling of the users' data uploading scheme, UAV trajectory, and allocation of communication and sensing time. However, the problem is a mixed integer nonlinear programming (MINLP) problem that is difficult to solve. To deal with the problem, we propose a two-stage alternating iterative optimization algorithm (AIOA) framework to find a proper solution. Specifically, in the first stage, we employ the successive convex approximation (SCA) algorithm to optimize the UAV trajectory. In the second stage, with fixed UAV trajectory, the block coordinate descent (BCD) technique is utilized to obtain a time allocation strategy and users' data upload scheme. Eventually, simulation experiments validate the effectiveness of the AIOA and its superiority compared to other benchmarks regarding the amount of data collected. The main contributions of this paper are as follows:

- We investigate a sensing-enabled integrated SAG data collection network, in which the UAV can not only work singly to sense data from multiple targets but also collaborate with the LEO satellite to collect communication data from multiple users.
- We design an optimization problem to maximize the total amount of data collected in the network, while simultaneously meet the constraints of UAV. We solve this problem by jointly optimizing the scheduling of the users' data uploading scheme, UAV trajectory, and allocation of communication and sensing time.
- We propose an effective two-stage AIOA framework to find a proper solution to the formulated problem. Specifically, in the first stage, we employ the SCA algorithm to optimize the UAV trajectory. Once the UAV trajectory is determined, the BCD technique is utilized in the second stage to obtain a strategy of time allocation and scheduling of users' data upload scheme.
- We conduct extensive simulation experiments validate the effectiveness of the AIOA and its superiority compared to other benchmarks regarding the amount of data collected.

II. System Model

In this section, we first introduce the network model of SAG networks, and then describe the data collection in multi-user multi-target scenarios. After that, we detail the data collections of communication and sensing.

A. Network Model

As shown in Fig. 1, we consider an integrated SAG data collection network, where the UAV and the LEO satellite are used to cooperatively collect data from N communication users (CUs) and M sensing targets. Let $\mathcal{C} \triangleq \{c_1, \cdots, c_n, \cdots, c_N\}$ and $\mathcal{S} \triangleq \{s_1, \cdots, s_m, \cdots, s_M\}$ denote the sets of CUs and sensing targets, respectively. In this network, the memory and energy limited UAV is sent to collect data from user c_n and target s_m according to a designed trajectory. Specifically, two

Authorized licensed use limited to: Aristotle University of Thessaloniki. Downloaded on September 23,2024 at 10:14:54 UTC from IEEE Xplore. Restrictions apply.
© 2024 IEEE. Personal use is permitted, but republication/redistribution requires IEEE permission. See https://www.ieee.org/publications/rights/index.html for more information.

This article has been accepted for publication in IEEE Journal on Selected Areas in Communications. This is the author's version which has not been fully edited and content may change prior to final publication. Citation information: DOI 10.1109/JSAC.2024.3459079

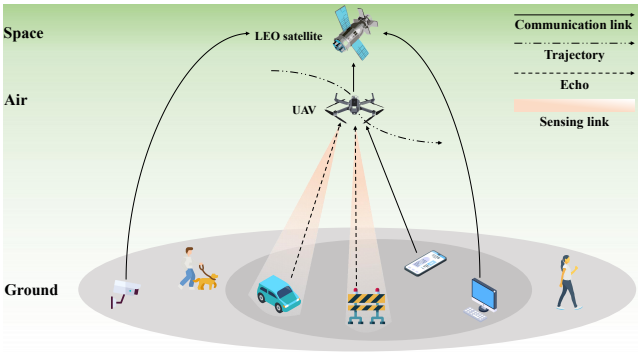

Fig. 1. Illustration of SAG networks for the collection of communication data and sensing data.

types of data need to be collected, namely, communication data and sensing data. For the communication data collection, the UAV serves as an air base station or relay to assist the LEO satellite in data collection, i.e. c_n can upload its data directly to the LEO satellite or indirectly through the UAV. For sensing data collection, the UAV serves as a radar to sense data from the target s_m, such as information about the target's position, velocity, and shape, as well as information about the target's attitude. Although the UAV shows great flexibility in data collection, only some users and targets can establish wireless connections with the UAV for data collection due to limited service coverage. Let $\mathcal{C}' \subseteq \mathcal{C}$ and $\mathcal{S}' \subseteq \mathcal{S}$ denote the subsets of users and targets of the UAV's service coverage, respectively. For users outside the set $\mathcal{C}'$, they can only upload data directly to the LEO satellite. For targets outside the set $\mathcal{S}'$, the UAV will not be able to collect data from them.

In this network, we assume that user c_n and target s_m are stationary [1] on the ground while the UAV is flying at a constant altitude H [30]. Consequently, the positions of the user c_n, the target s_m, and the UAV are modeled using the two-dimensional Cartesian coordinate. Let $\mathbf{a}_n = [x_n, y_n]^T$, $\mathbf{b}_m = [x_m, y_m]^T$, and $\mathbf{q} = [x_u, y_u]^T$ denote the coordinates of user c_n, target s_m, and UAV, respectively. Note that the positions of all users and targets are known in advance to facilitate the design of the UAV trajectory. Subsequently, the data collection in multi-user multi-target scenarios is presented.

B. Data Collection in Multi-user Multi-target Scenarios

We adopt a path discretization approach to model the UAV's flight state [19], which requires fewer variables to represent the flight state compared to the conventional time-slot division method. As illustrated in Fig. 2, the UAV's flight distance is composed of $K+2$ waypoints defined as $\left\{\mathbf{q}_k = [x_k^u, y_k^u]^T \mid 0 \le k \le K+1, k \in \mathbf{Z}_+\right\}$, where $\mathbf{q}_k$ is the coordinate of the k-th waypoint, and $\mathbf{q}_0$ and $\mathbf{q}_{K+1}$ denote the known initial and final waypoints of UAV, respectively. Among the $K+2$ waypoints, there are $K+1$ line segments, and we use $\mathbf{\Delta}_k = \mathbf{q}_{k+1} - \mathbf{q}_k$ to denote the k-th segment. Similar to the conventional time-slot division method, the UAV remains stationary at segment $\mathbf{\Delta}_k$, and it should meet the distance constraint, given by

$$\|\mathbf{\Delta}_k\| \le \min\left\{d_{max}, v_{max} t_k\right\}, \tag{1}$$

where $\|\cdot\|$ returns the Euclidean distance, d_{max} represents the maximum distance in each segment, $v_{\max}$ is the UAV maximum speed, and t_k denotes the duration of segment $\mathbf{\Delta}_k$. For each segment, there are up to four schemes for data collection, which are presented as follows:

- Upload to UAV (UAV scheme): User c_n uploads its data to the UAV, and the data is stored in the UAV.
- Upload to LEO satellite (Direct scheme): User c_n directly uploads its data to the LEO satellite.
- Upload to LEO satellite (Relaying scheme): User c_n uploads its data to the LEO satellite with the help of the UAV.
- Sensed by UAV (Sensing scheme): The UAV actively sends perception signals to the sensing target s_m and acquires sensing data from the echoes.

Note that for each segment of the UAV trajectory, time division multiple access (TDMA) is employed among the N CUs and M sensing targets. Let $\beta_{n,k}$ and $\alpha_{m,k}$ denote the time allocated for the user c_n to upload data, and that allocated for the UAV to sense the target s_m at the segment $\mathbf{\Delta}_k$, respectively. Then, the time allocation constraint is given by

$$\sum_{s_m \in \mathcal{S}} \alpha_{m,k} + \sum_{g_n \in \mathcal{C}} \beta_{n,k} \le t_k. \tag{2}$$

Additionally, in one flight, the UAV trajectory $\mathbf{Q}$ is comprised of the $K+2$ waypoints, given by

$$\mathbf{Q} = [\mathbf{q}_0, \cdots, \mathbf{q}_k, \cdots, \mathbf{q}_{K+1}]. \tag{3}$$

At the segment $\mathbf{\Delta}_k$, the distances from the UAV to user c_n and that to target s_m are, respectively, written as

$$d_{n,k} = \sqrt{\|\mathbf{q}_k - \mathbf{a}_n\|^2 + H^2}, \tag{4}$$

$$d_{m,k} = \sqrt{\|\mathbf{q}_k - \mathbf{b}_m\|^2 + H^2}. \tag{5}$$

Note that the coordinate of segment $\mathbf{\Delta}_k$ is defined as the coordinate of its initial position. In the next subsection, we detail the data collections of communication and sensing.

C. Data Collections of Communication and Sensing

Recall that there are up to four data collection schemes on the network in each segment, with the UAV and LEO satellite collecting data in TDMA mode, meaning that each user has only one time slot. For the first three data collection schemes, each user schedules up to one scheme to upload data. To simplify the description, we use three binary variables $x_{n,k}^{\mathrm{I}}$, $x_{n,k}^{\mathrm{II}}$, and $x_{n,k}^{\mathrm{III}}$ to represent these three schemes. For example,

[1] In this paper, we assume that users and targets are stationary, simplifying the system model. Dynamic scenarios may introduce some changes on the system, such as the mobility management, which involves the localization and movement prediction of users and targets. In addition, dynamic scenarios may need real-time optimization for UAVs in the system, posing higher demands on the problem formulation and algorithmic complexity. On the other hand, it should be noted that the system optimization in dynamic scenarios may involve the analysis and optimization in static scenarios of this work, which can serve as an important reference. In future work, we will investigate such dynamic scenarios involving unknown trajectories of users and targets.

Authorized licensed use limited to: Aristotle University of Thessaloniki. Downloaded on September 23,2024 at 10:14:54 UTC from IEEE Xplore. Restrictions apply.
© 2024 IEEE. Personal use is permitted, but republication/redistribution requires IEEE permission. See https://www.ieee.org/publications/rights/index.html for more information.

This article has been accepted for publication in IEEE Journal on Selected Areas in Communications. This is the author's version which has not been fully edited and content may change prior to final publication. Citation information: DOI 10.1109/JSAC.2024.3459079

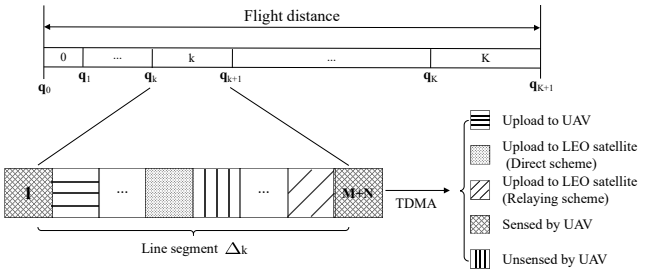

Fig. 2. Data collection in multi-user multi-target scenarios.

$x^{\mathrm{I}}_{n,k} = 1$ means that the UAV scheme is used for user c_n to upload data at segment $\boldsymbol{\Delta}k$, or not otherwise. The same logic applies to the other two schemas. So there is a natural constraint, given by

$$\begin{aligned} &x^{\mathrm{I}}_{n,k} + x^{\mathrm{II}}_{n,k} + x^{\mathrm{III}}_{n,k} \leq 1, \\ &x^{j}_{n,k} \in \{0,1\}\,,\ j \in \{\mathrm{I},\mathrm{II},\mathrm{III}\}\,. \end{aligned} \tag{6}$$

Next, we will discuss in detail the data collection process through user upload and UAV sensing.

1) Upload to UAV (UAV scheme) with $x^{I}_{n,k} = 1$: In this scheme, the data is uploaded to the UAV by user c_n and stored at the UAV. Then, the amount of data collected is given by

$$R^{\mathrm{I}}_{n,k} = \beta_{n,k} B_{\mathrm{I}} \log_2\left(1 + \frac{p_n \left|h_{n,k}\right|^2}{\sigma^2}\right), \tag{7}$$

where B_{I} represents the channel bandwidth of the c_n-UAV link, p_n is the transmit power of user c_n, σ^2 is the variance of the additive white Gaussian noise (AWGN), and $\left|h_{n,k}\right|^2$ represents the instantaneous channel gain between user c_n and the UAV at segment $\boldsymbol{\Delta}_k$. According to [31], we model the wireless channel as a LoS link, and the instantaneous channel gain is

$$\left|h_{n,k}\right|^2 = \frac{N_0}{d^2_{n,k}}, \tag{8}$$

where $N_0 = \frac{G_t G_c \lambda^2}{(4\pi)^2}$ is the reference channel gain per unit distance for the CU-UAV link, in which G_t and G_c denote the transmit and receive antenna gains, respectively, and λ represents the wavelength.

2) Upload to LEO satellite (Direct scheme) with $x^{II}_{n,k} = 1$: In this scheme, user c_n directly uploads its data to the LEO satellite. For this scheme, the achievable upload data rate of user c_n at segment $\boldsymbol{\Delta}_k$ is obtained as

$$r^{\mathrm{II}}_{n,k} = B_{\mathrm{II}} \log_2\left(1 + f(c_1) p_n\right), \tag{9}$$

where B_{II} is the channel bandwidth of the c_n-LEO satellite link, and $f(c_1)$ represents the fading coefficient under channel condition c_1 [32]. Here, we adopt the three-state condition model [33], where $f(c)$ equals 1.0, 3.46, and 5.03, corresponding to the bad, medium, and good conditions depending on the weather, respectively. In this scheme, the amount of data collected is $R^{\mathrm{II}}_{n,k} = \beta_{n,k} r^{\mathrm{II}}_{n,k}$.

3) Upload to LEO satellite (Relaying scheme) with $x^{III}_{n,k} = 1$: In this scheme, user c_n uploads its data to the LEO satellite with the help of the UAV, where the UAV serves as a half-duplex decode-and-forward (DF) relay to forward the user's data to the LEO satellite. For this scheme, the achievable upload data rate between user c_n and the LEO satellite at segment $\boldsymbol{\Delta}_k$ is

$$r^{\mathrm{III}}_{n,k} = \frac{1}{2} \min\left(B_{\mathrm{I}} \log_2\left(1 + \frac{p_n \left|h_{n,k}\right|^2}{\sigma^2}\right), r_u\right), \tag{10}$$

with

$$r_u = B_{\mathrm{III}} \log_2\left(1 + f(c_2) p_u\right), \tag{11}$$

where r_u is the achievable rate of the UAV-LEO satellite link, B_{III} and c_2 are the corresponding channel bandwidth of the satellite and channel condition of the UAV-LEO satellite link, and $\frac{1}{2}$ comes from the two-phase data transmission. Although the upload data rate of this scheme depends on the minimum upload rate of the two-hop link, in practice, the first-hop link tends to be worse than the second-hop link in terms of upload data rate. This often happens as the satellite communication can utilize the microwave band, which has a wide available bandwidth, thus B_{III} is much larger than B_{I} [12], [34]. Therefore, the upload data rate under this scheme is mainly limited by the first hop, i.e., $r^{\mathrm{III}}_{n,k} = \frac{1}{2} B_{\mathrm{I}} \log_2\left(1 + \frac{p_n |h_{n,k}|^2}{\sigma^2}\right)$, leading to that the amount of data collected is $R^{\mathrm{III}}_{n,k} = \beta_{n,k} r^{\mathrm{III}}_{n,k}$.

Comparing UAV scheme and Relaying scheme, we can see that for this collaborative data collection network, if a user is within the set $\mathcal{C}'$ and meanwhile the UAV has enough memory to store the data, then UAV scheme tends to be used for data collection because the data rate of UAV scheme is about twice that of Relaying scheme. On the contrary, when the amount of data stored in the UAV reaches its capacity limit, the Relaying scheme tends to be used for data collection.

4) Sensed by UAV (Sensing scheme): In this scheme, the UAV actively sends perception signals to the sensing target and acquires sensing data from the echoes. In this way, the radar estimation information rate is used to measure the sensing performance [24], [27], [28]. According to [24], the amount of data sensed from target s_m at segment $\boldsymbol{\Delta}_k$ is expressed as

$$R^{s}_{m,k} = \frac{1}{2} \alpha_{m,k} B_{\mathrm{I}} \log_2\left(1 + \frac{2 B_{\mathrm{I}} \mu \gamma^2 B^2_{\mathrm{I}} \sigma^2_{pre} p_s \left|h^{s}_{m,k}\right|^2}{\sigma^2}\right)^{\frac{\delta}{\mu B_{\mathrm{I}}}}, \tag{12}$$

where p_s is the UAV sensing power, μ is the radar pulse duration, γ is a constant determined by the shape of the radar waveform's power spectral density, σ^2_{pre} is the variance of the predicted radar return, and δ is the radar duty factor. Besides, $\left|h^{s}_{m,k}\right|^2$ is the channel gain of the radar detection link from target s_m to the UAV at segment $\boldsymbol{\Delta}_k$, given by

$$\left|h^{s}_{m,k}\right|^2 = \frac{N_1}{d^4_{m,k}}, \tag{13}$$

where $N_1 = \frac{G_t G_r \lambda^2 \epsilon}{(4\pi)^3}$ is the reference channel gain per unit distance of the UAV-target-UAV link similar to (8), in which

Authorized licensed use limited to: Aristotle University of Thessaloniki. Downloaded on September 23,2024 at 10:14:54 UTC from IEEE Xplore. Restrictions apply.
© 2024 IEEE. Personal use is permitted, but republication/redistribution requires IEEE permission. See https://www.ieee.org/publications/rights/index.html for more information.

This article has been accepted for publication in IEEE Journal on Selected Areas in Communications. This is the author's version which has not been fully edited and content may change prior to final publication. Citation information: DOI 10.1109/JSAC.2024.3459079

G_r is the UAV radar receiver antenna gain and ϵ is the radar cross-section [21].

III. Problem Formulation

In this section, we elaborate on the optimization problem, along with relevant constraints, aimed at maximizing the total amount of data collected.

A. Constraint Analysis

First, we detail the previously mentioned subsets $\mathcal{C}'$ and $\mathcal{S}'$ based on the received SNR. Whether a user or target belongs to the $\mathcal{C}'$ or $\mathcal{S}'$ subset depends on whether the corresponding received signal-to-noise ratio satisfies a predefined threshold. Mathematically, the received communication SNR $\Phi^c_{n,k}$, from the user $c_n \in \mathcal{C}'$ to the UAV at segment $\mathbf{\Delta}_k$, should satisfy

$$\Phi^c_{n,k} = \frac{p_n \left|h_{n,k}\right|^2}{\sigma^2} \geq \Phi^c_{th}, \tag{14}$$

where Φ^c_{th} is the predetermined communication SNR threshold. Equivalently, (14) can be expressed as

$$\left\|\mathbf{q}_k - \mathbf{a}_n\right\|^2 \leq \frac{N_0 p_n}{\Phi^c_{th}\sigma^2} - H^2. \tag{15}$$

Thus, at segment $\mathbf{\Delta}_k$, subset $\mathcal{C}'$ can be given by

$$\mathcal{C}'_k = \left\{ g_n \in \mathcal{C} \mid \left\|\mathbf{q}_k - \mathbf{a}_n\right\|^2 \leq \frac{N_0 p_n}{\Phi^c_{th}\sigma^2} - H^2 \right\}. \tag{16}$$

To facilitate the description of all segments, we denote the above relationship as a binary variable $c_{n,k}$, given by

$$c_{n,k} = \begin{cases} 1, & \text{If } \left\|\mathbf{q}_k - \mathbf{a}_n\right\|^2 \leq \frac{N_0 p_n}{\Phi^c_{th}\sigma^2} - H^2 \\ 0, & \text{Else} \end{cases} \tag{17}$$

where $c_{n,k} = 1$ indicates that user c_n can upload its data by the assistance of the UAV at segment $\mathbf{\Delta}_k$, while $c_{n,k} = 0$ indicates that the UAV cannot serve user c_n. In sight of the above, (6) can be rewritten as

$$\begin{aligned} &\begin{cases} x^{\mathrm{I}}_{n,k} + x^{\mathrm{II}}_{n,k} + x^{\mathrm{III}}_{n,k} = 1, & \text{If } c_{n,k} = 1 \\ x^{\mathrm{I}}_{n,k} = 0, x^{\mathrm{II}}_{n,k} = 1, x^{\mathrm{III}}_{n,k} = 0, & \text{Else} \end{cases} \\ &x^j_{n,k} \in \{0,1\}\,,\ j \in \{\mathrm{I},\mathrm{II},\mathrm{III}\}\,. \end{aligned} \tag{18}$$

Similar to (14), the sensing SNR $\Phi^s_{m,k}$, from the UAV to target $s_m \in \mathcal{S}'$ and back to the UAV at segment $\mathbf{\Delta}_k$, should satisfy

$$\Phi^s_{m,k} = \frac{N_2 \left|h^s_{m,k}\right|^2}{\sigma^2} \geq \Phi^s_{th}, \tag{19}$$

with

$$N_2 = 2B_{\mathrm{I}}\mu\gamma^2 B^2_{\mathrm{I}}\sigma^2_{pre}p_s, \tag{20}$$

where Φ^s_{th} is the predetermined sensing SNR threshold. And (19) is equivalent to

$$\left\|\mathbf{q}_k - \mathbf{b}_m\right\|^2 \leq \sqrt{\frac{N_2 N_1}{\Phi^s_{th}\sigma^2}} - H^2, \tag{21}$$

and thus, the subset $\mathcal{S}'_k$ is given by

$$\mathcal{S}'_k = \left\{ s_m \in \mathcal{S} \mid \left\|\mathbf{q}_k - \mathbf{b}_m\right\|^2 \leq \sqrt{\frac{N_2 N_1}{\Phi^s_{th}\sigma^2}} - H^2 \right\}. \tag{22}$$

Similar to (17), we use a binary variable $s_{m,k}$ to represent the above relationship of all segments, given by

$$s_{m,k} = \begin{cases} 1, & \text{If } \left\|\mathbf{q}_k - \mathbf{b}_m\right\|^2 \leq \sqrt{\frac{N_2 N_1 p_s}{\Phi^s_{th}\sigma^2}} - H^2 \\ 0, & \text{Else} \end{cases} \tag{23}$$

where $s_{m,k} = 1$ indicates that the UAV is able to sense data from s_m at segment $\mathbf{\Delta}_k$, or fails otherwise.

Second, in order to ensure fairness among users, i.e., each user should achieve a minimum upload data amount Q_n, denoted as (24), which is at the top of the next page. Moreover, in practice, the radar estimation information rate is normally lower than the upload data rate [24]. To ensure that a sufficient amount of data sensed is collected, the amount of data sensed per target needs to satisfy a constraint, which is given by

$$\sum_{k=0}^{K} s_{m,k} R^s_{m,k} \geq Q^s_m, \tag{25}$$

where Q^s_m is the minimum sensing data amount per target. Besides, there is a time limit for the whole data collection process. In other words, there is a maximum flight time limit for the UAV. Specifically, the UAV's prolonged flight not only depletes the energy it carries, leading to loss of control and safety accidents, but also increases the temperature of the UAV's fuselage, affecting the functioning of its key components, and in turn reducing flight stability. Thus, the time limit is given by

$$\sum_{k=0}^{K} t_k \leq T_{th}, \tag{26}$$

where T_{th} is the duration of data collection.

In particular, we should emphasize the limitations of the UAV in terms of power consumption and energy consumption and storage capacity. On the one hand, due to the finite battery capacity in practice, UAVs are not capable of continuous flight. Specifically, the energy consumption of UAVs mainly comes from three aspects: flight, communication, and sensing, of which flight is the largest contributor. Therefore, the other two aspects of energy consumption can be ignored [21], and the constraint on the total energy consumption of the UAV should follow the mathematical form given by

$$\sum_{k=0}^{K} t_k p^f_k \leq E_{th}, \tag{27}$$

where E_{th} is the threshold of the UAV energy consumption. p^f_k indicates the propulsion power for flight during segment $\mathbf{\Delta}_k$ [19], given by

$$\begin{aligned} p^f_k = {} & P_0\left(1 + \frac{3v_k^2}{U^2_{\mathrm{tip}}}\right) + P_s\left(\sqrt{1 + \frac{v_k^4}{4v_0^4}} - \frac{v_k^2}{2v_0^2}\right)^{1/2} \\ & + \frac{1}{2} d_0 \varpi_0 s_0 A_0 v_k^3, \end{aligned} \tag{28}$$

Authorized licensed use limited to: Aristotle University of Thessaloniki. Downloaded on September 23,2024 at 10:14:54 UTC from IEEE Xplore. Restrictions apply.
© 2024 IEEE. Personal use is permitted, but republication/redistribution requires IEEE permission. See https://www.ieee.org/publications/rights/index.html for more information.

This article has been accepted for publication in IEEE Journal on Selected Areas in Communications. This is the author's version which has not been fully edited and content may change prior to final publication. Citation information: DOI 10.1109/JSAC.2024.3459079

$$\sum_{k=0}^{K}\left(c_{n,k}\left(x_{n,k}^{\mathrm{I}}R_{n,k}^{\mathrm{I}}+x_{n,k}^{\mathrm{II}}R_{n,k}^{\mathrm{II}}+x_{n,k}^{\mathrm{III}}R_{n,k}^{\mathrm{III}}\right)+\left(1-c_{n,k}\right)R_{n,k}^{\mathrm{II}}\right)\geq Q_n. \tag{24}$$

where $v_k \triangleq \frac{|\mathbf{q}k+1-\mathbf{q}k|}{t_k}$ represents the UAV speed at segment $\mathbf{\Delta}_k$. Notations P_0 and U_{tip} denote the blade profile power of hovering status and tip speed of the UAV rotor blade, respectively. Moreover, P_s and v_0 represent the blade induced power and mean rotor induced velocity in UAV hovering status, respectively. Additionally, d_0, s_0, ϖ_0, and A_0 correspond to the fuselage drag ratio, rotor robustness, air density, and rotor disk area, respectively. On the other hand, it should be confirmed that the total amount of data uploaded by the users (when $x_{n,k}^{\mathrm{I}}=1$) and sensed from the targets will not exceed the memory capacity of the UAV. This can be done by satisfying the constraint, given by

$$Q_u=\sum_{k=0}^{K}\left(\sum_{n=1}^{N}c_{n,k}x_{n,k}^{\mathrm{I}}R_{n,k}^{\mathrm{I}}+\sum_{m=1}^{M}s_{m,k}R_{m,k}^{s}\right)\leq Q_u^{th}, \tag{29}$$

where Q_u^{th} is the threshold of the UAV memory capacity. The initial and final positions in a UAV flight trajectory are assumed to be known and are denoted by $\mathbf{q}_I$ and $\mathbf{q}_F$, respectively, given by

$$\mathbf{q}_0=\mathbf{q}_I,\ \mathbf{q}_{K+1}=\mathbf{q}_F. \tag{30}$$

Overall, all constraints in the collaborative SAG data collection network have been described, and the main notations are summarized in Table I for readability.

TABLE I: Main Notations Summary

Notation	Definition
$\mathcal{C}$, $\mathcal{S}$	Set of communication users and sensing targets
$\mathcal{C}'$, $\mathcal{S}'$	Set of users and targets within UAV service coverage
N, M	Number of communication users and sensing targets
c_n, s_m	n-th communication user and m-th sensing target
$\mathbf{\Delta}_k$	k-th segment
$\mathbf{a}_n$, $\mathbf{b}_m$, $\mathbf{q}_k$	Coordinate of user c_n, target s_m, and the UAV at segment $\mathbf{\Delta}_k$
H	UAV flight altitude
$K+2$	Number of waypoints
$d_{\max}$	Maximum distance of each segment
$v_{\max}$	UAV maximum speed
t_k	Duration of segment $\mathbf{\Delta}_k$
$\beta_{n,k}$, $\alpha_{m,k}$	Time allocated variables
$\mathbf{Q}$	UAV trajectory
$d_{n,k}$, $d_{m,k}$	Distance from the UAV to user c_n and that to target s_m at segment $\mathbf{\Delta}_k$
$x_{n,k}^{\mathrm{I}}$, $x_{n,k}^{\mathrm{II}}$, $x_{n,k}^{\mathrm{III}}$	Scheme scheduling variables
$R_{n,k}^{\mathrm{I}}$, $R_{n,k}^{\mathrm{II}}$, $R_{n,k}^{\mathrm{III}}$	Amount of data collected from c_n at segment $\mathbf{\Delta}_k$ with different scheduling
B_{I}, B_{II}, B_{III}	Channel bandwidth
p_n, p_s, p_u	Transmit power
$h_{n,k}$, $h_{m,k}^{s}$	Channel parameter of the UAV-c_n link and the UAV-s_m link
σ^2	Noise power
N_0, N_1	Reference channel gain per unit distance for the CU-UAV link and UAV-target-UAV link
$f(c)$	Fading coefficient of satellite link under channel condition c
Φ_{th}^{c}, Φ_{th}^{s}	Predetermined communication and sensing SNR threshold
$c_{n,k}$, $s_{m,k}$	Indicator variable about sets $\mathcal{C}'$ and $\mathcal{S}'$
Q_n, Q_m^{s},	Minimum upload data amount per user and minimum sensing data amount per target
Q_u^{th}, Q_{sys}	UAV memory capacity and the total amount of data collected
T_{th}, E_{th}	Duration of data collection and threshold of the UAV energy consumption
$\mathbf{q}_I$, $\mathbf{q}_F$	Initial and final positions in the UAV flight trajectory

B. Problem Formulation

We aim to maximize the total amount of data collected in the SAG data collection network, denoted by Q_{sys} as follows,

$$\begin{aligned}Q_{\text{sys}}=&\underbrace{\sum_{k=0}^{K}\sum_{n=1}^{N}c_{n,k}\left(x_{n,k}^{\mathrm{I}}R_{n,k}^{\mathrm{I}}+x_{n,k}^{\mathrm{II}}R_{n,k}^{\mathrm{II}}+x_{n,k}^{\mathrm{III}}R_{n,k}^{\mathrm{III}}\right)}_{Q_1}\\&+\underbrace{\sum_{k=0}^{K}\sum_{n=1}^{N}\left(1-c_{n,k}\right)R_{n,k}^{\mathrm{II}}}_{Q_2}+\underbrace{\sum_{k=0}^{K}\sum_{m=1}^{M}s_{m,k}R_{m,k}^{s}}_{Q_3}.\end{aligned} \tag{31}$$

Note that Q_{sys} consists three parts. The first part Q_1 represents the total amount of data uploaded from users within the set $\mathcal{C}'$, the second part Q_2 represents the total amount of data uploaded from users out of set $\mathcal{C}'$, and the third part Q_3 represents the total amount of data sensed by the UAV.

Based on the previous analysis, we design a system optimization problem with the objective of maximizing the amount of data collected [35]–[37]. This involves optimizing the UAV trajectory, time allocation and data upload scheduling, formulated by

$$\begin{aligned}\mathbf{P0}:\quad&\max_{\mathcal{V}}\quad Q_{\text{sys}}\\&\text{s.t.}\quad (1),(2),(17),(18),(23),\\&\qquad (24),(25),(26),(27),(29),(30),\end{aligned} \tag{32}$$

where $\mathcal{V}=\left\{\mathbf{q}_k,t_k,c_{n,k},s_{m,k},\alpha_{m,k},\beta_{n,k},x_{n,k}^{\mathrm{I}},x_{n,k}^{\mathrm{II}},x_{n,k}^{\mathrm{III}}\right\}$ is the set of the optimization variables, in which $0\leq k\leq K+1$, $c_n\in\mathcal{C}$, and $s_m\in\mathcal{S}$.

After observing the optimization problem **P0**, we notice that there is coupling among the variables, resulting in a non-convex problem. In addition, the optimization of the UAV trajectory increases the complexity of the problem, and the inclusion of discrete variables further complicates the analysis.

Authorized licensed use limited to: Aristotle University of Thessaloniki. Downloaded on September 23,2024 at 10:14:54 UTC from IEEE Xplore. Restrictions apply.
© 2024 IEEE. Personal use is permitted, but republication/redistribution requires IEEE permission. See https://www.ieee.org/publications/rights/index.html for more information.

This article has been accepted for publication in IEEE Journal on Selected Areas in Communications. This is the author's version which has not been fully edited and content may change prior to final publication. Citation information: DOI 10.1109/JSAC.2024.3459079

As a result of these factors, the **P0** problem evolves into a MINLP problem. Several approaches have been proposed to solve such problems, the most recent of which is the deep reinforcement learning (DRL) algorithm [38]. However, although the DRL algorithm shows unrivaled potential in handling such problems, the algorithm has several challenges in both the design phase and the training phase. Specifically, in the design phase of the algorithm, it faces complicated design problems regarding the huge state space and action space, while the sparse reward design problem is also a challenge. In addition, the design of the UAV trajectory also becomes a hurdle. In the training phase of the algorithm, it also will meet the problems of high training cost and unstable training [39]. Therefore, we develop an AIOA based on the BCD technique to solve the optimization problem **P0**, which will be detailed in the next section.

IV. Proposed Method

In this section, we first utilize the BCD technique to decompose the problem **P0**, resulting into two subproblems. Next, we analyze each subproblem individually, and based on these analyses, we proceed to design the AIOA framework to solve the problem **P0**.

A. Problem Decomposition

In this subsection, we decompose the original problem **P0** by using the BCD technique into two subproblems **P1** and **P2**, given by

$$\begin{aligned} \mathbf{P1}: \quad & \max_{\mathcal{V}_1} \quad Q_{\text{sys}} \\ \text{s.t.} \quad & (1),(2),(17),(18),(23),(24), \\ & (25),(26),(27),(29),(30), \end{aligned} \tag{33}$$

where $\mathcal{V}_1 = \{t_k, \mathbf{q}_k, c_{n,k}, s_{m,k}\}$, and

$$\begin{aligned} \mathbf{P2}: \quad & \max_{\mathcal{V}_2} \quad Q_{\text{sys}} \\ \text{s.t.} \quad & (2),(18),(24),(25),(29), \end{aligned} \tag{34}$$

where $\mathcal{V}_2 = \left\{\alpha_{m,k}, \beta_{n,k}, x^{\text{I}}_{n,k}, x^{\text{II}}_{n,k}, x^{\text{III}}_{n,k}\right\}$. Note that subproblem **P1** focuses on optimizing the UAV trajectory with a given $\mathcal{V}_2$ and obtains a $\mathcal{V}_1$. Then, the subproblem **P2** focuses on optimizing the data upload scheduling scheme and time allocation strategy with a given $\mathcal{V}_1$ and obtains a $\mathcal{V}_2$. By alternately iterating these two subproblems, we can efficiently find a proper solution to the problem **P0**.

Next, we detail the solution process for **P1** and **P2**.

B. Solutions

1) Solving P1: In **P1**, we observe that the variables $c_{n,k}$ and $s_{m,k}$ are not only binary but also coupled with $\mathbf{q}_k$, while the objective function and constraints in (24), (25), (27), and (29) are non-convex, making it very difficult to solve. To address **P1**, we first employ the big-M method to reconstruct the non-convex parts [40], and then solve the non-convex constraints by the SCA algorithm.

We start to solve **P1** with restructuring the constraints in (17) and (23). Specifically, to use big-M method with the constraints in (17) and (23), we introduce two slack variables $\xi_{1,n,k}$ and $\xi_{2,m,k}$, such that

$$\xi_{1,n,k} \geq \|\mathbf{q}_k - \mathbf{a}_n\|^2, \ \xi_{2,m,k} \geq \|\mathbf{q}_k - \mathbf{b}_m\|^2, \tag{35}$$

and the constraints in (17) and (23) are converted to

$$c_{n,k} = \begin{cases} 1, & \text{If } \xi_{1,n,k} \leq \frac{N_0 p_n}{\Phi^c_{th}\sigma^2} - H^2 \\ 0, & \text{Else} \end{cases} \tag{36}$$

and

$$s_{m,k} = \begin{cases} 1, & \text{If } \xi_{2,m,k} \leq \sqrt{\frac{N_2 N_1}{\Phi^s_{th}\sigma^2}} - H^2 \\ 0. & \text{Else} \end{cases} \tag{37}$$

Then, according to the big-M method, the constraints in (36) and (37) can be rewritten as

$$\begin{cases} \xi_{1,n,k} - \mathbb{M}(1 - c_{n,k}) \leq N_3 < \xi_{1,n,k} + \mathbb{M}c_{n,k}, \\ \xi_{2,m,k} - \mathbb{M}(1 - s_{m,k}) \leq N_4 < \xi_{2,m,k} + \mathbb{M}s_{m,k}, \\ c_{n,k} \in \{0,1\}, \ s_{m,k} \in \{0,1\}, \end{cases} \tag{38}$$

where

$$N_3 = \frac{N_0 p_n}{\Phi^c_{th}\sigma^2} - H^2, \ N_4 = \sqrt{\frac{N_1 N_2}{\Phi^s_{th}\sigma^2}} - H^2, \tag{39}$$

and $\mathbb{M}$ is a sufficiently large constant.

Second, based on the converted constraints in (35) and (38), we can restructure and handle the non-convex functions in **P1**. Specifically, for the non-convex UAV capacity constraint in (29), we introduce another two slack variables $\xi_{3,n,k}$ and $\xi_{4,m,k}$, such that

$$\begin{aligned} \xi_{3,n,k} &\geq x^{\text{I}}_{n,k} R^{\text{I}}_{n,k} \\ &= x^{\text{I}}_{n,k}\beta_{n,k}B_1 \log_2\left(1 + \frac{p_n N_0}{\sigma^2\left(\|\mathbf{q}_k - \mathbf{a}_n\|^2 + H^2\right)}\right), \end{aligned} \tag{40}$$

and

$$\begin{aligned} \xi_{4,m,k} &\geq R^s_{m,k} \\ &= \alpha_{m,k}\frac{\delta}{2\mu}\log_2\left(1 + \frac{N_2 N_1}{\sigma^2\left(\|\mathbf{q}_k - \mathbf{b}_m\|^2 + H^2\right)^2}\right). \end{aligned} \tag{41}$$

Then, the constraint in (29) can be rewritten as

$$\sum_{k=0}^{K}\left(\sum_{n=1}^{N} c_{n,k}\xi_{3,n,k} + \sum_{m=1}^{M} s_{m,k}\xi_{4,m,k}\right) \leq Q^{th}_u. \tag{42}$$

By employing the big-M method, (42) can be rewritten as

$$\begin{cases} \sum_{k=0}^{K}\left(\sum_{n=1}^{N}\xi_{5,n,k} + \sum_{m=1}^{M}\xi_{6,m,k}\right) \leq Q^{th}_u, \\ \xi_{3,n,k} - \mathbb{M}\left(1 - c_{n,k}\right) \leq \xi_{5,n,k} \leq \xi_{3,n,k} + \mathbb{M}\left(1 - c_{n,k}\right), \\ \xi_{4,m,k} - \mathbb{M}\left(1 - s_{m,k}\right) \leq \xi_{6,m,k} \leq \xi_{4,m,k} + \mathbb{M}\left(1 - s_{m,k}\right), \\ -\mathbb{M}c_{n,k} \leq \xi_{5,n,k} \leq \mathbb{M}c_{n,k}, \\ -\mathbb{M}s_{m,k} \leq \xi_{6,m,k} \leq \mathbb{M}s_{m,k}, \end{cases} \tag{43}$$

where $\xi_{5,n,k}$ and $\xi_{6,m,k}$ are auxiliary variables. However, the constraint in (29) is still non-convex due to newly introduced

Authorized licensed use limited to: Aristotle University of Thessaloniki. Downloaded on September 23,2024 at 10:14:54 UTC from IEEE Xplore. Restrictions apply.
© 2024 IEEE. Personal use is permitted, but republication/redistribution requires IEEE permission. See https://www.ieee.org/publications/rights/index.html for more information.

This article has been accepted for publication in IEEE Journal on Selected Areas in Communications. This is the author's version which has not been fully edited and content may change prior to final publication. Citation information: DOI 10.1109/JSAC.2024.3459079

constraints in (40) and (41). To handle this issue, we introduce slack variables $\xi_{7,n,k}$ and $\xi_{8,m,k}$ to (40) and (41), such that

$$\xi_{7,n,k} \leq \|\mathbf{q}_k - \mathbf{a}_n\|^2 + H^2, \tag{44}$$

$$\xi_{8,m,k} \leq \left(\|\mathbf{q}_k - \mathbf{b}_m\|^2 + H^2\right)^2, \tag{45}$$

and the constraints in (40) and (41) can be rewritten as

$$\xi_{3,n,k} \geq x^{\mathrm{I}}_{n,k}\beta_{n,k}B_1 \log_2\left(1 + \frac{p_n N_0}{\sigma^2 \xi_{7,n,k}}\right), \tag{46}$$

$$\xi_{4,m,k} \geq \alpha_{m,k}\frac{\delta}{2\mu}\log_2\left(1 + \frac{N_2 N_1}{\sigma^2 \xi_{8,m,k}}\right). \tag{47}$$

It is not difficult to find that the constraint in (29) has been decoupled and the constraints except (44) and (45) are convex. While, in the non-convex constraints (44) and (45), the right-hand-side (RHS) of each constraint is a convex function with respect to $\mathbf{q}_k$, and the global concave lower bound of the RHS can be obtained based on any given localized point $\mathbf{q}_k^i$ in the i-th iteration by the SCA algorithm. Specifically, by using the fact that first-order Taylor expansion is a global lower bound of a convex function, the lower bounds of the RHS of (44) and (45) can be denoted as

$$\begin{aligned}&\|\mathbf{q}_k - \mathbf{a}_n\|^2 + H^2 \geq \left\|\mathbf{q}_k^i - \mathbf{a}_n\right\|^2 + \\ &2\left(\mathbf{q}_k^i - \mathbf{a}_n\right)^T\left(\mathbf{q}_k - \mathbf{q}_k^i\right) + H^2 \geq \xi_{7,n,k},\end{aligned} \tag{48}$$

and

$$\begin{aligned}&\left(\|\mathbf{q}_k - \mathbf{b}_m\|^2 + H^2\right)^2 \geq \left(\left\|\mathbf{q}_k^i - \mathbf{b}_m\right\|^2 + H^2\right)^2 + \\ &4\left(\left\|\mathbf{q}_k^i - \mathbf{b}_m\right\|^2 + H^2\right)\left(\mathbf{q}_k^i - \mathbf{b}_m\right)^T\left(\mathbf{q}_k - \mathbf{q}_k^i\right) \geq \xi_{8,m,k}.\end{aligned} \tag{49}$$

For the non-convex constraints in (24) and (25) and non-concave objective function, we use the same method mentioned above. Specifically, we introduce slack variables, such as

$$\begin{aligned}\tau_{1,n,k} &\leq x^{\mathrm{I}}_{n,k}R^{\mathrm{I}}_{n,k} + x^{\mathrm{II}}_{n,k}R^{\mathrm{II}}_{n,k} + x^{\mathrm{III}}_{n,k}R^{\mathrm{III}}_{n,k} \\ &= \left(x^{\mathrm{I}}_{n,k} + \frac{1}{2}x^{\mathrm{III}}_{n,k}\right)\beta_{n,k}B_1 \times \\ &\quad \log_2\left(1 + \frac{p_n N_0}{\sigma^2\left(\|\mathbf{q}_k - \mathbf{a}_n\|^2 + H^2\right)}\right) \\ &\quad + x^{\mathrm{II}}_{n,k}R^{\mathrm{II}}_{n,k} \triangleq R_{n,k},\end{aligned} \tag{50}$$

and

$$\begin{aligned}\tau_{2,m,k} &\leq R^s_{m,k} \\ &= \frac{1}{2}\alpha_{m,k}\frac{\delta}{\mu}\log_2\left(1 + \frac{N_2 N_1}{\sigma^2\left(\|\mathbf{q}_k - \mathbf{b}_m\|^2 + H^2\right)^2}\right).\end{aligned} \tag{51}$$

With the above manipulations, the non-convex constraints in (24) and (25), and non-concave objective function of problem **P1** can be rewritten as

$$\sum_{k=0}^{K}\left(c_{n,k}\tau_{1,n,k} + (1 - c_{n,k})R^{\mathrm{II}}_{n,k}\right) \geq Q_n, \tag{52}$$

$$\sum_{k=0}^{K} s_{m,k}\tau_{2,m,k} \geq Q^s_m, \tag{53}$$

and

$$\begin{aligned}&\sum_{k=0}^{K}\sum_{n=1}^{N}\left(c_{n,k}\tau_{1,n,k} + (1 - c_{n,k})R^{\mathrm{II}}_{n,k}\right) \\ &+ \sum_{k=0}^{K}\sum_{m=1}^{M} s_{m,k}\tau_{2,m,k} \triangleq \breve{Q^{\mathrm{sys}}}.\end{aligned} \tag{54}$$

Similar to (42), we can rewrite (52), (53) and $\hat{Q}_{\mathrm{sys}}$ by the big-M method as

$$\begin{cases}\displaystyle\sum_{k=0}^{K}\tau_{3,n,k} \geq Q_n, \\ \tau_{1,n,k} - \mathbb{M}(1 - c_{n,k}) \leq \tau_{3,n,k} \leq \tau_{1,n,k} + \mathbb{M}(1 - c_{n,k}), \\ R^{\mathrm{II}}_{n,k} - \mathbb{M}c_{n,k} \leq \tau_{3,n,k} \leq R^{\mathrm{II}}_{n,k} + \mathbb{M}c_{n,k},\end{cases} \tag{55}$$

$$\begin{cases}\displaystyle\sum_{k=0}^{K}\tau_{4,m,k} \geq Q^s_m, \\ \tau_{2,m,k} - \mathbb{M}(1 - s_{m,k}) \leq \tau_{4,m,k} \leq \tau_{2,m,k} + \mathbb{M}(1 - s_{m,k}), \\ -\mathbb{M}s_{m,k} \leq \tau_{4,m,k} \leq \mathbb{M}s_{m,k},\end{cases} \tag{56}$$

and

$$\sum_{k=0}^{K}\sum_{n=1}^{N}\tau_{3,n,k} + \sum_{k=0}^{K}\sum_{m=1}^{M}\tau_{4,m,k} \triangleq Q^{lb}_{\mathrm{sys}}, \tag{57}$$

where $\tau_{3,n,k}$ and $\tau_{4,m,k}$ are auxiliary variables. Although we have achieved the decoupling of variables by reconstructing (24), (25) and the objective function through the big-M method, the newly introduced constraints in (50) and (51) are still non-convex. We adopt the SCA algorithm to address this issue. Specifically, similar to (48) and (49), the lower bounds are obtained by using the first-order Taylor expansion [19], and then (50) and (51) can be rewritten as

$$\begin{aligned}R_{n,k} \geq &\left(x^{\mathrm{I}}_{n,k} + \frac{1}{2}x^{\mathrm{III}}_{n,k}\right)\beta_{n,k}B_{\mathrm{I}} \times \\ &\left(N_5 - N_6\left(\|\mathbf{q}_k - \mathbf{a}_n\|^2 - \left\|\mathbf{q}_k^i - \mathbf{a}_n\right\|^2\right)\right) \\ &+ x^{\mathrm{II}}_{n,k}R^{\mathrm{II}}_{n,k} \geq \tau_{1,n,k},\end{aligned} \tag{58}$$

and

$$\begin{aligned}R^s_{m,k} \geq &\alpha_{m,k}\frac{\delta}{2\mu} \times \\ &\left(N_7 - N_8\left(\|\mathbf{q}_k - \mathbf{b}_n\|^2 - \left\|\mathbf{q}_k^i - \mathbf{b}_n\right\|^2\right)\right) \geq \tau_{2,m,k},\end{aligned} \tag{59}$$

Authorized licensed use limited to: Aristotle University of Thessaloniki. Downloaded on September 23,2024 at 10:14:54 UTC from IEEE Xplore. Restrictions apply.
© 2024 IEEE. Personal use is permitted, but republication/redistribution requires IEEE permission. See https://www.ieee.org/publications/rights/index.html for more information.

This article has been accepted for publication in IEEE Journal on Selected Areas in Communications. This is the author's version which has not been fully edited and content may change prior to final publication. Citation information: DOI 10.1109/JSAC.2024.3459079

where

$$\begin{cases} N_5 = \log_2\left(1+\dfrac{p_n N_0/\sigma^2}{\left\|\mathbf{q}_k^i-\mathbf{a}_n\right\|^2+H^2}\right), \\ N_6 = \dfrac{p_n N_0/\sigma^2/\left(\left\|\mathbf{q}_k^i-\mathbf{a}_n\right\|^2+H^2\right)^2}{\ln 2\left(1+\frac{p_n N_0/\sigma^2}{\left\|\mathbf{q}_k^i-\mathbf{a}_n\right\|^2+H^2}\right)}, \\ N_7 = \log_2\left(1+\dfrac{N_2 N_1/\sigma^2}{\left(\left\|\mathbf{q}_k^i-\mathbf{b}_n\right\|^2+H^2\right)^2}\right), \\ N_8 = \dfrac{2N_2N_1/\sigma^2/\left(\ln 2\left(\left\|\mathbf{q}_k^i-\mathbf{b}_n\right\|^2+H^2\right)\right)}{\left(N_2N_1/\sigma^2+\left(\left\|\mathbf{q}_k^i-\mathbf{b}_n\right\|^2+H^2\right)^2\right)}. \end{cases} \tag{60}$$

Therefore, the variables in the constraints (24), (25), (29) and objective function have been decoupled, and the derived non-convex constraints have been solved by the SCA algorithm. However, the problem **P1** remains intractable because of the existence of the UAV energy constraint in (27). Fortunately, an effective solution to this problem has been proposed in [19]. Specifically, a relaxed upper bound has been used in the second term of (27), such as

$$\begin{aligned} G_k &\geq t_k\left(\sqrt{1+\frac{v_k^4}{4v_0^4}}-\frac{v_k^2}{2v_0^2}\right)^{1/2} \\ &= \sqrt{\sqrt{t_k^4+\frac{\left\|\mathbf{q}_{k+1}-\mathbf{q}_k\right\|^4}{4v_0^4}}-\frac{\left\|\mathbf{q}_{k+1}-\mathbf{q}_k\right\|^2}{2v_0^2}}, \end{aligned} \tag{61}$$

where G_k is a slack variable, and the constraint in (27) is rewritten as

$$\sum_{k=0}^{K} P_0 t_k\left(1+\frac{3v_k^2}{U_{\text{tip}}^2}\right)+P_s G_k+\frac{1}{2}d_0\varpi_0 s_0 A_0 t_k v_k^3 \leq E_{th}. \tag{62}$$

While, (61) is equivalent to

$$G_k^2+\frac{\left\|\mathbf{q}_{k+1}-\mathbf{q}_k\right\|^2}{v_0^2} \geq \frac{t_k^4}{G_k^2}. \tag{63}$$

For the non-convex constraint in (63), the left-hand-side (LHS) is a convex function with respect to G_k and $\mathbf{q}_k$, and RHS is a convex function with respect to t_k and G_k. Thus, the global lower bound of the LHS in (63) can be given by the first-order Taylor expansion, which is

$$\begin{aligned} &G_k^2+\frac{\left\|\mathbf{q}_{k+1}-\mathbf{q}_k\right\|^2}{v_0^2} \geq \left(G_k^i\right)^2+2G_k^i\left(G_k-G_k^i\right) \\ &+\frac{1}{v_0^2}\left(2\left(\mathbf{q}_{k+1}^i-\mathbf{q}_k^i\right)^T\left(\mathbf{q}_{k+1}-\mathbf{q}_k\right)-\left\|\mathbf{q}_{k+1}^i-\mathbf{q}_k^i\right\|^2\right) \\ &\geq \frac{t_k^4}{G_k^2}, \end{aligned} \tag{64}$$

where G_k^i is the given localized point in the i-th iteration.

Algorithm 1: The proposed UAV trajectory optimization algorithm.

Input $\mathcal{V}_2$;
Initialize iterative number $i=0$, convergence accuracy θ_1, and objective value $Q_{\text{sys}}^i=0$;
Initialize UAV trajectory $\{\mathbf{q}_k\}$ as $\{\mathbf{q}_k^i\}$;
Initialize $\{G_k\}$ as $\{G_k^i\}$;
repeat
  $i=i+1$;
  Solve the problem **P1-1** with the given $\mathcal{V}_2$, $\{\mathbf{q}_k^{i-1}\}$, and $\{G_k^{i-1}\}$, and denote partial solutions as $\{\mathbf{q}_k^*\}$ and $\{G_k^*\}$;
  Compute Q_{sys}^{lb} as $Q_{\text{sys}}^{lb,i}$;
  Let $\{\mathbf{q}_k^i\}=\{\mathbf{q}_k^*\}$ and $\{G_k^i\}=\{G_k^*\}$;
until $\left|Q_{sys}^{lb,i}-Q_{sys}^{lb,i-1}\right|/Q_{sys}^{lb,i} \leq \theta_1$;
return $\left\{t_k, \mathbf{q}_k^i, c_{n,k}, s_{m,k}\right\}$

In the end, problem **P1** can be rewritten as follows,

$$\begin{aligned} \textbf{P1-1}: \quad & \max_{\mathcal{V}_{1-1}} \quad Q_{\text{sys}}^{lb} \\ \text{s.t.} \quad & (1),(2),(18),(26),(30),(35),(38), \\ & (43),(46)-(49),(55)-(59),(62),(64), \end{aligned} \tag{65}$$

where $\mathcal{V}_{1-1}=\{t_k,\mathbf{q}_k,c_{n,k},s_{m,k},\xi_1-\xi_8,\tau_1-\tau_4,G_k\}$.

Overall, problem **P1** has been transformed from a MINLP problem to a mixed-integer convex optimization problem **P1-1** with binary variables $c_{n,k}$ and $s_{m,k}$. Fortunately, **P1-1** can be transformed into a convex optimization problem by traditional branch-and-bound or variable relaxation method, and then solved by a convex optimization solver such as MOSEK. Based on this, we propose a UAV trajectory optimization algorithm as shown in Algorithm 1, where G_k can be initialized by making the left and right hand sides of (61) equal according to the given $\mathbf{q}_k$ and t_k. The above procedure is performed during each iteration until convergence.

*2) Solving **P2**:* Although problem **P2** is a mixed integer programming problem involving binary variables $x_{n,k}^{\text{I}}$, $x_{n,k}^{\text{II}}$, and $x_{n,k}^{\text{III}}$, we can solve it by relaxing the integer variables to continuous real variables from 0 to 1. Thus, (18) can be converted to

$$\begin{aligned} &\begin{cases} x_{n,k}^{\text{I}}+x_{n,k}^{\text{II}}+x_{n,k}^{\text{III}}=1, & \text{If } c_{n,k}=1 \\ x_{n,k}^{\text{I}}=0, x_{n,k}^{\text{II}}=1, x_{n,k}^{\text{III}}=0, & \text{Else} \end{cases} \\ &x_{n,k}^{j} \in [0,1]\,,\ j \in \{\text{I},\text{II},\text{III}\}\,. \end{aligned} \tag{66}$$

Note that this relaxation removes the integer optimization, thus making the problem more tractable [41].

Then, **P2** can be relaxed as follows:

$$\begin{aligned} \tilde{\textbf{P2}}: \quad & \max_{\mathcal{V}_2} \quad Q_{\text{sys}} \\ \text{s.t.} \quad & (2),(24),(25),(29),(66). \end{aligned} \tag{67}$$

However, $\tilde{\textbf{P2}}$ is still non-convex because of the high coupling among the variables. To solve this problem, we also use the

Authorized licensed use limited to: Aristotle University of Thessaloniki. Downloaded on September 23,2024 at 10:14:54 UTC from IEEE Xplore. Restrictions apply.
© 2024 IEEE. Personal use is permitted, but republication/redistribution requires IEEE permission. See https://www.ieee.org/publications/rights/index.html for more information.

This article has been accepted for publication in IEEE Journal on Selected Areas in Communications. This is the author's version which has not been fully edited and content may change prior to final publication. Citation information: DOI 10.1109/JSAC.2024.3459079

Algorithm 2: The proposed algorithm for **P2**.

Input $\mathcal{V}_1$;
Initialize convergence accuracy θ_2, $\mathcal{V}_4$, Q_{sys}^1 and Q_{sys}^2;
repeat
  Solve the problem **P2-1** with the given $\mathcal{V}_1$ and $\mathcal{V}_4$, and obtain $\mathcal{V}_3$;
  Compute Q_{sys} as Q_{sys}^1;
  Solve the problem **P2-2** with the given $\mathcal{V}_1$ and $\mathcal{V}_3$, and obtain $\mathcal{V}_4$;
  Compute Q_{sys} as Q_{sys}^2;
until $\left|Q_{sys}^2 - Q_{sys}^1\right| / Q_{sys}^2 \leq \theta_2$;
return $\left\{\alpha_{m,k}, \beta_{n,k}, x_{n,k}^{I}, x_{n,k}^{II}, x_{n,k}^{III}\right\}$

Algorithm 3: The proposed BCD based AIOA framework.

Initialize $\mathcal{V}_2$, iterative number $I = 0$, and maximum number of iterations $I_{\max}$;
while $I < I_{max}$ **do**
  Solve the problem **P1-1** with the given $\mathcal{V}_2$ by Algorithm 1;
  Solve the problem $\tilde{\mathbf{P2}}$ with the given $\mathcal{V}_1$ by Algorithm 2;
  $I = I + 1$;
end
return $\mathcal{V}_1$, $\mathcal{V}_2$

BCD technique for $\tilde{\mathbf{P2}}$. Specifically, the problem $\tilde{\mathbf{P2}}$ can be decomposed into the subproblems **P2-1** and **P2-2**, given by

$$\begin{aligned} \textbf{P2-1}: \quad & \max_{\mathcal{V}_3} \quad Q_{\text{sys}} \\ \text{s.t.} \quad & (24), (29), (66), \end{aligned} \tag{68}$$

where $\mathcal{V}_3 = \left\{x_{n,k}^{\text{I}}, x_{n,k}^{\text{II}}, x_{n,k}^{\text{III}}\right\}$, and

$$\begin{aligned} \textbf{P2-2}: \quad & \max_{\mathcal{V}_4} \quad Q_{\text{sys}} \\ \text{s.t.} \quad & (2), (24), (25), (29), \end{aligned} \tag{69}$$

where $\mathcal{V}_4 = \{\alpha_{m,k}, \beta_{n,k}\}$. The problems **P2-1** and **P2-2** are linear optimization problems with respect to the corresponding variables, which can be solved easily by means of several convex tools, such as CVX. By alternately solving the problems **P2-1** and **P2-2**, we can obtain a time allocation strategy and a data upload scheduling scheme. The details are shown in Algorithm 2.

C. Design of AIOA based on BCD technique

Now, we present the AIOA framework to solve the problem **P0** with the objective of obtaining a locally optimal solution for $\mathcal{V}$. The specific steps of the framework are detailed in Algorithm 3. Specifically, in step 3 of the Algorithm 3, we solve **P1-1** with the given $\mathcal{V}_2$ in each iteration while updating the local points, until the algorithm converges to finally return $\mathcal{V}_1$. Similarly, in step 4 of algorithm 3, we aim to solve **P2** with the given $\mathcal{V}_1$, in which we solve **P2-1** and **P2-2** alternately until the algorithm converges and $\mathcal{V}_2$ is finally obtained. It is worth noting that the convergence of AIOA can be guaranteed by varying the initial points, and its convergence analysis is similar to the work in [42]–[44]. Additionally, unlike existing methods, our proposed AIOA framework deals with complicated nonconvex optimization problems mainly through AO and SCA. This approach leads to an optimized solution in each subproblem, eventually yielding an appropriate solution to the original problem, which is often applicable to problems with a well-defined structure.

The computational complexity of Algorithm 3 can be analyzed as follows. As Algorithm 3 is composed of Algorithms 1 and 2, we first analyze the computational complexity of Algorithms 1 and 2. For Algorithm 1, its computational complexity is $\mathcal{O}\left(J_1\left((K+2)\left(7\left(M+N\right)+3\right)\right)^{3.5}\right)$, where $(K+2)\left(7\left(M+N\right)+3\right)$ represents the number of variables and J_1 is the number of iterations required [43]. For Algorithm 2, its computational complexity mainly lies in steps 4 and 6. Specifically, the complexity of step 4 is $\mathcal{O}\left(\left(3\left(K+2\right)N\right)^{3.5}\right)$, and the complexity of step 6 is $\mathcal{O}\left(\left(\left(K+2\right)\left(M+N\right)\right)^{3.5}\right)$. Thus, the computational complexity of Algorithm 2 is $\mathcal{O}\left(J_2\left(\left(3\left(K+2\right)N\right)^{3.5} + \left(\left(K+2\right)\left(M+N\right)\right)^{3.5}\right)\right)$, where J_2 denotes the number of iterations required for convergence in Algorithm 2 [43]. In summary, the computational complexity of Algorithm 3 can be given by

$$\mathcal{O}\Bigg(I_{\max}\Bigg(J_1\left(\left(K+2\right)\left(7\left(M+N\right)+3\right)\right)^{3.5} + J_2\Bigg(\left(3N(K+2)\right)^{3.5} + \left(\left(K+2\right)(M+N)\right)^{3.5}\Bigg)\Bigg)\Bigg). \tag{70}$$

V. Simulation Results and Discussions

A. Parameter Settings

This part presents some general simulation parameter settings. If not specified, the number of communication users and sensing targets are both set to two, where the locations of users are $[20, 80]^T$ m and $[80, 80]^T$ m, while the locations of targets are $[40, 30]^T$ m and $[60, 30]^T$ m. The UAV's initial and final locations are $\mathbf{q}_I = [0, 50]^T$ m and $\mathbf{q}_F = [100, 50]^T$ m. The UAV flight altitude H is 100 m, and its maximum speed is 30 m/s. Moreover, the wireless bandwidth B_{I} and B_{II} are set to 1 MHz and 10 MHz, while the transmit power at each user is set to 0.1 W, with the noise variance σ^2 set to -110 dBm. The channel gain per unit distance for the CU-UAV and UAV-target-UAV links is -60 dB. In further, for the parameters related to the radar estimation information rate in (12), we follow the settings in [27], where the UAV sensing power p_s is 10 W. Meanwhile, for the parameters related to the UAV propulsion power in (28), we follow the settings in [19]. Furthermore, the minimum amount of upload data per user Q_n is 10 Mbits, while the minimum amount of sensing data per target Q_m^s is 10 Kbits. The UAV memory capacity Q_u^{th} is 100 Mbits, the duration of data collection T_{th} is 30 s, and the

Authorized licensed use limited to: Aristotle University of Thessaloniki. Downloaded on September 23,2024 at 10:14:54 UTC from IEEE Xplore. Restrictions apply.
© 2024 IEEE. Personal use is permitted, but republication/redistribution requires IEEE permission. See https://www.ieee.org/publications/rights/index.html for more information.

This article has been accepted for publication in IEEE Journal on Selected Areas in Communications. This is the author's version which has not been fully edited and content may change prior to final publication. Citation information: DOI 10.1109/JSAC.2024.3459079

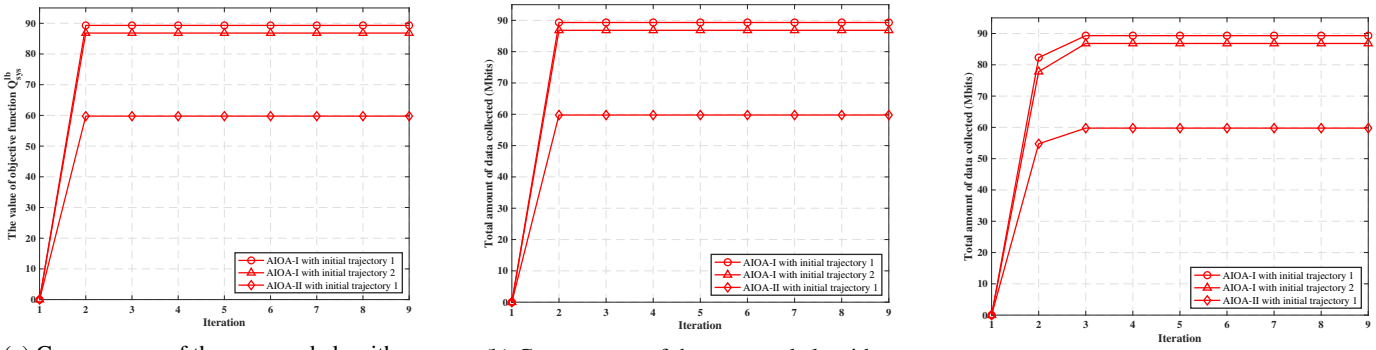

(a) Convergence of the proposed algorithm 1 in the AIOA's last iteration.

(b) Convergence of the proposed algorithm 2 in the AIOA's last iteration.

(c) Convergence of the AIOA.

Fig. 3. Convergence of AIOA and internal algorithms under different settings.

TABLE II: Main Parameter Settings

Parameters	**Value**
UAV flight altitude H	100 m
UAV maximum speed $v_{\max}$	30 m/s
Wireless bandwidth B_{I} and B_{II}	1 MHz, 10 MHz
Transmit power at users	0.1 W
Noise variance σ^2	-110 dBm
Average channel gain N_0 and N_1	-60 dB
UAV sensing power p_s	10 W
Minimum amount of upload data per user Q_n	10 Mbits
Minimum amount of sensing data per target Q_m^s	10 Kbits
UAV memory capacity Q_u^{th}	100 Mbits
Duration of data collection T_{th}	30 s
Energy consumption threshold E_{th}	10 kJ

energy consumption threshold E_{th} is 10 kJ, respectively. In the end, the carrier frequency of the CU-UAV link and UAV-target-UAV link is C-band with 5 GHz, while the carrier frequency of CU-LEO satellite link and UAV-LEO satellite link is Ka-band with 35 GHz. For convenience, the main parameter settings are summarized in Table II.

B. Simulation Results

In this subsection, we verify the effectiveness of the proposed AIOA using two criteria regarding UAV coverage. In addition, we provide several data collection schemes for comparison. For convenience, we use the following notations to denote the schemes:

- **AIOA-I**: The proposed AIOA framework with a wider UAV coverage optimizes the UAV trajectory, time allocation, and scheduling of data uploading, where $\sqrt{N_3} = \sqrt{N_4} = 65$ m.
- **AIOA-II**: The proposed AIOA framework with a narrow UAV coverage optimizes the UAV trajectory, time allocation, and scheduling of data uploading, where $\sqrt{N_3} = \sqrt{N_4} = 35$ m.
- All-LEO: All communication data are uploaded either directly to the LEO satellite (Direct scheme) or with the help of the UAV to the LEO satellite (Relaying scheme). In this scheme, except for variable $x_{n,k}^{\mathrm{I}}$, all the other variables are optimized.
- SF: The UAV flies straight from the initial position $\mathbf{q}_I$ to the final position $\mathbf{q}_F$ at a constant speed, where the data uploading schedule is random and the time allocation strategy is optimized in this scheme.
- Non-UAV: In this scheme, we aim to present the effect of satellite communication in our considered scenario. Therefore, in this competing scheme, users share the time resource to upload communication data, and the sensing mission is ignored.

Note that the coverage of the UAV in the All-LEO and SF is the same as that of AIOA-I. These competing schemes are the simplified versions of our proposed AIOA with lower complexity, which can provide some insights for the performance of our scheme. Besides, two initial trajectories are considered,

- Initial trajectory 1: This initial trajectory represents that $\{\mathbf{q}_k^0\}_{k=0}^{K+1}$ is a simple straight-line path from $\mathbf{q}_I$ to $\mathbf{q}_F$
- Initial trajectory 2: This initial trajectory is a complex M-shaped trajectory that starts from $\mathbf{q}_I$ and passes through the points $[20, 80]^T$ m, $[50, 30]^T$ m and $[80, 80]^T$ m in sequence, finally reaching $\mathbf{q}_F$.

Fig. 3 shows the convergence of our proposed AIOA framework and the internal Algorithms 1 and 2. From Fig. 3, we can observe that the AIOA and Algorithms 1, 2 all converge in just a few iterations, which proves the fast convergence rate and effectiveness. Moreover, in Fig. 3(c), "initial trajectory 1" performs better than "initial trajectory 2" in the case of AIOA-I, which highlights the importance of choosing a suitable initial solution. Thus, if not specified, we then default to "initial trajectory 1". In further, AIOA-I performs better than AIOA-II. Specifically, after several iterations, AIOA-I can collect about 90 Mbits of data, compared to AIOA-II, which can only collect about 60 Mbits, about 50% improvement in the amount collected by AIOA-I. This is because the UAV can collect data at a wider range.

Figs. 4 and 5 show the UAV trajectories and the corresponding speed changes. We can observe through these figures that the UAV generally flies at its highest speed toward the users and targets. This strategy is chosen not only to obtain better channel conditions but also because, in the AIOA-II, the UAV should be close to the user and the target to help the users collect data and sense the targets. Particularly, it is evident from Figs. 4(a), 5(a), 4(b), and 5(b) that "Initial Trajectory 2"

Authorized licensed use limited to: Aristotle University of Thessaloniki. Downloaded on September 23,2024 at 10:14:54 UTC from IEEE Xplore. Restrictions apply.
© 2024 IEEE. Personal use is permitted, but republication/redistribution requires IEEE permission. See https://www.ieee.org/publications/rights/index.html for more information.

This article has been accepted for publication in IEEE Journal on Selected Areas in Communications. This is the author's version which has not been fully edited and content may change prior to final publication. Citation information: DOI 10.1109/JSAC.2024.3459079

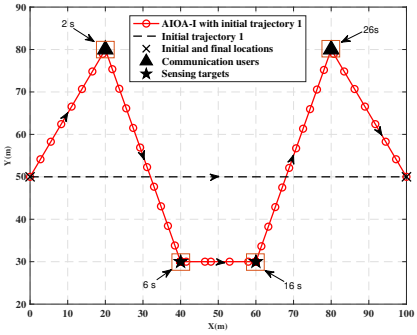

(a) UAV trajectory of AIOA-I with initial trajectory 1.

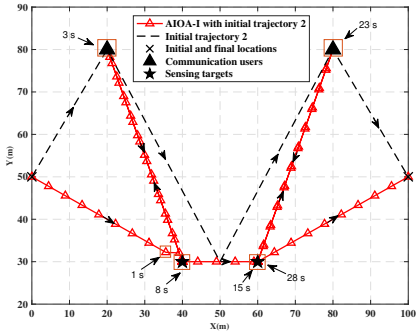

(b) UAV trajectory of AIOA-I with initial trajectory 2.

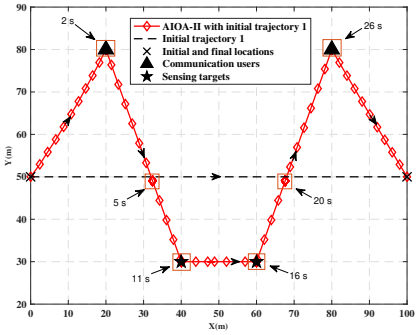

(c) UAV trajectory of AIOA-II with initial trajectory 1.

Fig. 4. UAV trajectories under different settings.

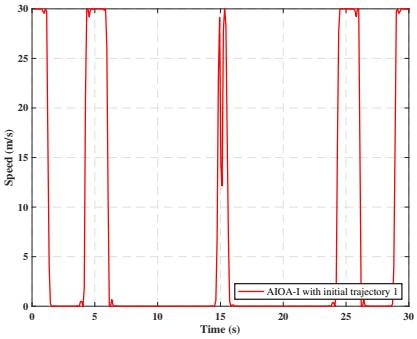

(a) UAV speed variation of AIOA-I with initial trajectory 1.

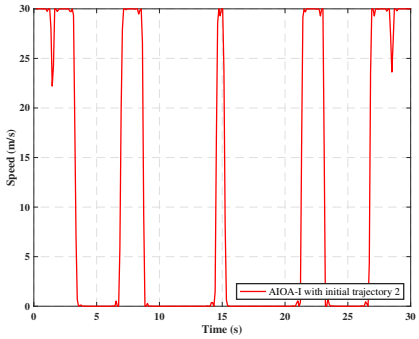

(b) UAV speed variation of AIOA-I with initial trajectory 2.

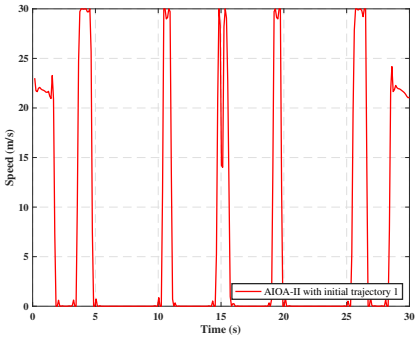

(c) UAV speed variation of AIOA-II with initial trajectory 1.

Fig. 5. UAV speed under different settings.

is characterized by a longer duration of flight as opposed to hovering over either the users or the targets. Consequently, this results in "Initial Trajectory 2" collecting less data compared to "Initial Trajectory 1" for a given threshold T_{th}. Moreover, while the trajectories in Figs. 4(a) and 4(c) appear deceptively similar, but notable differences emerge when examining the speed variations in Figs. 5(a) and 5(c). Specifically, Fig. 5(a) illustrates four hover points, i.e., moments when the speed is 0, contrasted with six such points in Fig. 5(c). This discrepancy is attributable to the limited service coverage of the UAV in AIOA-II, necessitating a balance in positioning between the users and targets for optimal data upload and target sensing, thereby maximizing Q_{sys}. However, such positions often entail suboptimal channel conditions compared to closer proximity to either the users or targets, which leads to AIOA-II collecting less data than AIOA-I.

Fig. 6 shows the impact of the UAV maximum speed $v_{\max}$ on Q_{sys}, where the speed ranges from 10 m/s to 30 m/s. Observing Fig. 6, it is evident that increasing the UAV's maximum speed $v_{\max}$ enhances Q_{sys} in all schemes except for the SF and Non-UAV schemes. This improvement occurs because a higher maximum speed allows the UAV to quickly approach users and targets, meeting the conditions of subsets $\mathcal{C}'$ and $\mathcal{S}'$, and gaining better channel gains. Moreover, the AIOA-I consistently outperforms AIOA-II. Specifically, as the UAV maximum speed increases, Q_{sys} of the AIOA-I increases

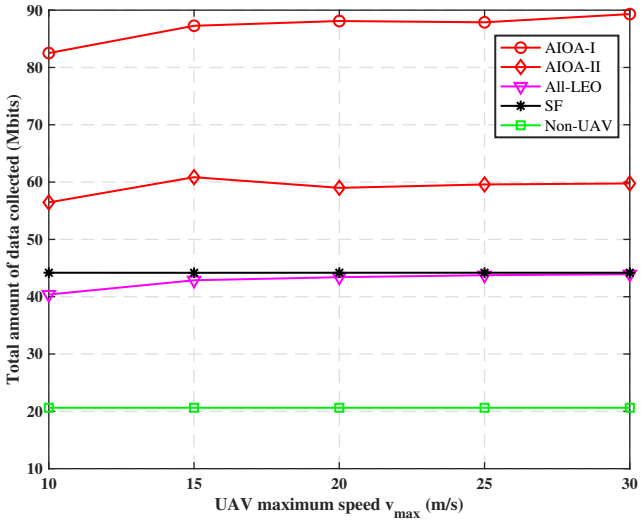

Fig. 6. Total amount of data collected versus $v_{\max}$.

roughly from 81 Mbits to 90 Mbits. In comparison, Q_{sys} of the AIOA-II only increases roughly from 57 Mbits to 60 Mbits. This is because, in the former, the UAV collects data farther from the users and targets. In addition, the proposed schemes, AIOA-I and AIOA-II outperform other data collection schemes by at least 38%, proving superior performance.

Fig. 7 shows the relationship between Q_{sys} and duration

Authorized licensed use limited to: Aristotle University of Thessaloniki. Downloaded on September 23,2024 at 10:14:54 UTC from IEEE Xplore. Restrictions apply.
© 2024 IEEE. Personal use is permitted, but republication/redistribution requires IEEE permission. See https://www.ieee.org/publications/rights/index.html for more information.

This article has been accepted for publication in IEEE Journal on Selected Areas in Communications. This is the author's version which has not been fully edited and content may change prior to final publication. Citation information: DOI 10.1109/JSAC.2024.3459079

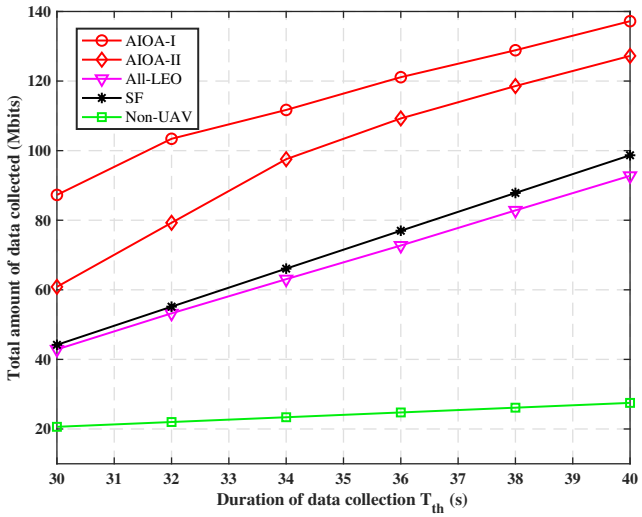

Fig. 7. Total amount of data collected versus T_{th}, where $v_{\max}$ is 15 m/s.

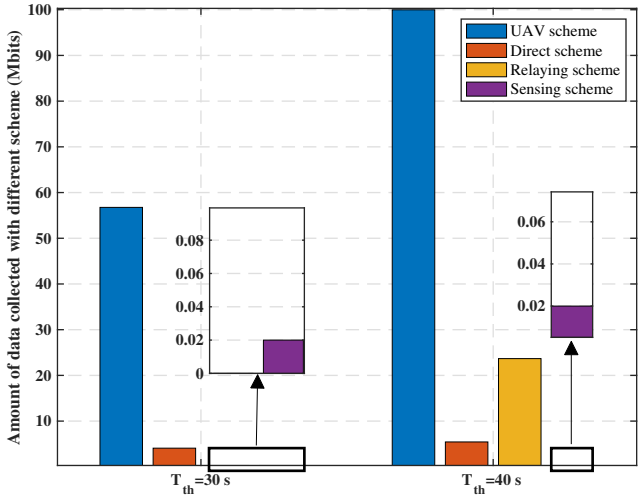

Fig. 8. Data collection of our proposed AIOA-II under various data upload schemes and durations.

T_{th} for different schemes, where T_{th} ranges from 30 s to 40 s and $v_{\max}$ is 15 m/s. Observing Fig. 7, we can see that with the increasing T_{th}, Q_{sys} with all schemes shows an increasing trend. In particular, the growth rates of Q_{sys} in the proposed schemes slow down when Q_{sys} reaches about 100 Mbits. Due to the fact that the UAV plays a core data collection role in the SAG network, and when Q_{sys} reaches the upper limit of 100 Mbits of UAV capacity, the UAV's role is limited, ultimately resulting in a slowdown in the growing trend of Q_{sys}. Moreover, the proposed schemes outperform other schemes for various T_{th}. Specifically, when T_{th} = 40 s, the Q_{sys} of All-LEO, SF, and Non-UAV schemes are approximately 92 Mbits, 100 Mbits, and 30 Mbits, respectively. In comparison, the Q_{sys} of AIOA-I and AIOA-II are 138 Mbits and 129 Mbits, respectively, showing the effectiveness of the AIOA scheme.

Fig. 8 illustrates the data collection capabilities of our proposed AIOA-II under various data upload schemes and durations T_{th}, where $T_{th} = \{30, 40\}$ s. To facilitate observation, the Direct scheme in Fig. 8 combines the data uploaded both inside and outside the set $\mathcal{C}'$, with the amount of data within $\mathcal{C}'$ being zero. At the duration of $T_{th} = 30$ s, the UAV scheme collects data approximately 56 Mbits, the Direct scheme collects about 4 Mbits, the Relaying scheme gathers 0 Mbits, and the Sensing scheme accumulates 20 Kbits. When the duration increases to $T_{th} = 40$ s, the amount of data collected by the UAV scheme rises to roughly 100 Mbits of UAV capacity, the Direct scheme collects about 6 Mbits, the Relaying scheme gathers 24 Mbits, while the Sensing scheme remains at 20 Kbits. From these numerical comparisons, we observe that within this sensing-assisted SAG integrated network, the UAV scheme is the first choice for data upload, followed by the Relaying scheme, and finally the Direct scheme.

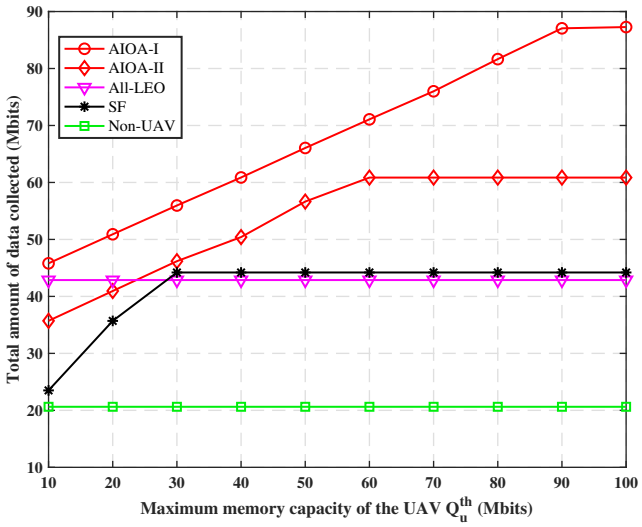

Fig. 9. Total amount of data collected versus Q_u^{th}, where $v_{\max}$ is 15 m/s.

Fig. 9 shows the impact of memory capacity of the UAV Q_u^{th} on the total collected data Q_{sys}, where Q_u^{th} varies from 10 Mbits to 100 Mbits and $v_{\max}$ is 15 m/s. We can observe from Fig. 9 that except for the All-LEO and Non-UAV schemes, Q_{sys} first increases and then stabilizes with the increase of Q_u^{th}. The reason is that when Q_u^{th} is small, the UAV memory capacity dominates the effect on Q_{sys}, and increasing Q_u^{th} can significantly increase Q_{sys}. However, when Q_u^{th} is large, the memory capacity constraint is negligible. Therefore, the performance gain of increasing Q_u^{th} on Q_{sys} becomes marginal. Moreover, the proposed AIOA outperforms other schemes with the increasing Q_u^{th}, which shows the effectiveness of the proposed AIOA. Besides, from Fig. 9, we perceive an interesting phenomenon that the Q_{sys} of the AIOA-II scheme is first lower and then higher than that of All-LEO when Q_u^{th} increases. This is due to the performance of the AIOA-II is limited by the service range, under a lower memory capacity Q_u^{th}. However, with a higher memory capacity Q_u^{th}, AIOA-II can take full advantage of these sufficient UAV memory resources to collect data, while the All-LEO scheme fails.

Fig. 10 shows the impact of Q_m^s on several aforementioned schemes' Q_{sys}, where Q_m^s ranges from 5 Kbits to 10 Kbits

Authorized licensed use limited to: Aristotle University of Thessaloniki. Downloaded on September 23,2024 at 10:14:54 UTC from IEEE Xplore. Restrictions apply.
© 2024 IEEE. Personal use is permitted, but republication/redistribution requires IEEE permission. See https://www.ieee.org/publications/rights/index.html for more information.

This article has been accepted for publication in IEEE Journal on Selected Areas in Communications. This is the author's version which has not been fully edited and content may change prior to final publication. Citation information: DOI 10.1109/JSAC.2024.3459079

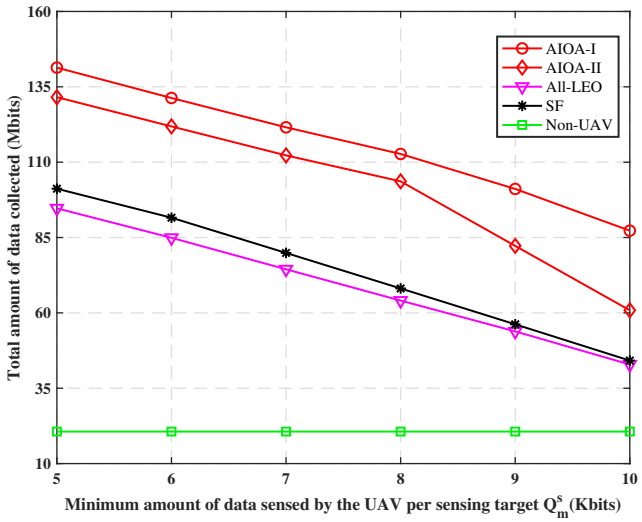

Fig. 10. Total amount of data collected versus Q_m^s, where $v_{\max}$ is 15 m/s.

and $v_{\max}$ is 15 m/s. It can be observed from Fig. 10 that, as Q_m^s increases, Q_{sys} of all schemes shows a declining trend, except the Non-UAV scheme. This can be attributed to the fact that the radar estimation information rate is significantly lower than the upload data rate. As a result, the UAV needs to allocate more time resource to sense the targets. When T_{th} is maintained at a constant value, the extended sensing duration results in a decrease of Q_{sys}. In particular, within the proposed schemes, there is an observable acceleration in the decrease rate of Q_{sys} when Q_m^s exceeds 8 Kbits, at which point Q_{sys} reaches the UAV memory capacity. This trend indicates that beyond the limitation of the UAV memory capacity, increasing demand for sensing amounts exerts a more pronounced impact on Q_{sys}. In addition, under different Q_m^s settings, the proposed schemes are better than the competing schemes, proving their effectiveness on data collection.

VI. Conclusion

In this paper, we considered a sensing-enabled integrated SAG data collection network in which the UAV could not only work alone to sense data from multiple targets, but also collaborate with the LEO satellite to collect communication data from multiple users. For this system, we first posed the optimization problem designed to maximize the total amount of data collected in the network while satisfying the constraints of UAV energy consumption, storage capacity, and minimum amount of sensor data per target. What's more, considering that the network included three layers and the UAV had dual functions of communication and sensing, this problem could be solved by jointly optimizing the scheduling of the users' data upload scheme, the UAV trajectory, and the allocation of communication and sensing time. We further designed the AIOA framework to find a feasible solution. Specifically, we alternately optimized the UAV trajectory, time allocation strategy, and data upload schedule in each iteration. Finally, simulation experiments validated the effectiveness of AIOA and its superiority over other benchmarks. In particular, the experimental results also showed that the AIOA was superior to the linear trajectories of the UAV in terms of the amount of data collected.

References

[1] W. Jiang, B. Han, M. A. Habibi, and H. D. Schotten, "The road towards 6G: A comprehensive survey," *IEEE Open J. Commun. Soc.*, vol. 2, pp. 334–366, 2021.

[2] S. Tang, Q. Yang, L. Fan, X. Lei, A. Nallanathan, and G. K. Karagiannidis, "Contrastive learning based semantic communications," *IEEE Trans. Commun.*, pp. 1–12, 2024.

[3] H. Hu, K. Xiong, G. Qu, Q. Ni, P. Fan, and K. B. Letaief, "AoI-minimal trajectory planning and data collection in UAV-assisted wireless powered iot networks," *IEEE Internet Things J.*, vol. 8, no. 2, pp. 1211–1223, 2021.

[4] L. Liu, K. Xiong, J. Cao, Y. Lu, P. Fan, and K. B. Letaief, "Average AoI minimization in UAV-assisted data collection with RF wireless power transfer: A deep reinforcement learning scheme," *IEEE Internet Things J.*, vol. 9, no. 7, pp. 5216–5228, 2022.

[5] Y. Liu, K. Xiong, Y. Lu, Q. Ni, P. Fan, and K. B. Letaief, "UAV-aided wireless power transfer and data collection in Rician fading," *IEEE J. Sel. Areas Commun.*, vol. 39, no. 10, pp. 3097–3113, 2021.

[6] L. Zhang, Y. Wu, L. Chen, L. Fan, and A. Nallanathan, "Scoring aided federated learning on long-tailed data for wireless IoMT based healthcare system," *IEEE J. Biomed. Health Informatics*, vol. 28, no. 6, pp. 3341–3348, 2024.

[7] L. Qu, G. Xu, Z. Zeng, N. Zhang, and Q. Zhang, "UAV-assisted RF/FSO relay system for space-air-ground integrated network: A performance analysis," *IEEE Trans. Wirel. Commun.*, vol. 21, no. 8, pp. 6211–6225, 2022.

[8] N. Cheng, H. Jingchao, Y. Zhisheng, Z. Conghao, W. Huaqing, L. Feng, Z. Haibo, and S. Xuemin, "6G service-oriented space-air-ground integrated network: A survey," *Chinese J. Aeronaut.*, vol. 35, no. 9, pp. 1–18, 2022.

[9] J. Sheng, X. Cai, Q. Li, C. Wu, B. Ai, Y. Wang, M. Kadoch, and P. Yu, "Space-air-ground integrated network development and applications in high-speed railways: A survey," *IEEE Trans. Intell. Transp. Syst.*, vol. 23, no. 8, pp. 10 066–10 085, 2022.

[10] D. Liu, J. Zhang, J. Cui, S. X. Ng, R. G. Maunder, and L. Hanzo, "Deep learning aided routing for space-air-ground integrated networks relying on real satellite, flight, and shipping data," *IEEE Wirel. Commun.*, vol. 29, no. 2, pp. 177–184, 2022.

[11] Y. Su, Y. Liu, Y. Zhou, J. Yuan, H. Cao, and J. Shi, "Broadband LEO satellite communications: Architectures and key technologies," *IEEE Wirel. Commun.*, vol. 26, no. 2, pp. 55–61, 2019.

[12] N. Dao, Q. Pham, N. H. Tu, T. T. Thanh, V. N. Q. Bao, D. S. Lakew, and S. Cho, "Survey on aerial radio access networks: Toward a comprehensive 6G access infrastructure," *IEEE Commun. Surv. Tutorials*, vol. 23, no. 2, pp. 1193–1225, 2021.

[13] O. Kodheli, E. Lagunas, N. Maturo, S. K. Sharma, B. Shankar, J. F. M. Montoya, J. C. M. Duncan, D. Spano, S. Chatzinotas, S. Kisseleff, J. Querol, L. Lei, T. X. Vu, and G. Goussetis, "Satellite communications in the new space era: A survey and future challenges," *IEEE Commun. Surv. Tutorials*, vol. 23, no. 1, pp. 70–109, 2021.

[14] R. Radhakrishnan, W. W. Edmonson, F. Afghah, R. M. Rodríguez-Osorio, F. Pinto, and S. C. Burleigh, "Survey of inter-satellite communication for small satellite systems: Physical layer to network layer view," *IEEE Commun. Surv. Tutorials*, vol. 18, no. 4, pp. 2442–2473, 2016.

[15] R. Samy, H. Yang, T. Rakia, and M. Alouini, "Space-air-ground FSO networks for high-throughput satellite communications," *IEEE Commun. Mag.*, vol. 61, no. 3, pp. 82–87, 2023.

[16] L. You, K. Li, J. Wang, X. Gao, X. Xia, and B. E. Ottersten, "Massive MIMO transmission for LEO satellite communications," *IEEE J. Sel. Areas Commun.*, vol. 38, no. 8, pp. 1851–1865, 2020.

[17] J. Shi, J. Hu, Y. Yue, X. Xue, W. Liang, and Z. Li, "Outage probability for OTFS based downlink LEO satellite communication," *IEEE Trans. Veh. Technol.*, vol. 71, no. 3, pp. 3355–3360, 2022.

[18] Y. Zeng and R. Zhang, "Energy-efficient UAV communication with trajectory optimization," *IEEE Trans. Wirel. Commun.*, vol. 16, no. 6, pp. 3747–3760, 2017.

[19] Y. Zeng, J. Xu, and R. Zhang, "Energy minimization for wireless communication with rotary-wing UAV," *IEEE Trans. Wirel. Commun.*, vol. 18, no. 4, pp. 2329–2345, 2019.

Authorized licensed use limited to: Aristotle University of Thessaloniki. Downloaded on September 23,2024 at 10:14:54 UTC from IEEE Xplore. Restrictions apply.
© 2024 IEEE. Personal use is permitted, but republication/redistribution requires IEEE permission. See https://www.ieee.org/publications/rights/index.html for more information.

This article has been accepted for publication in IEEE Journal on Selected Areas in Communications. This is the author's version which has not been fully edited and content may change prior to final publication. Citation information: DOI 10.1109/JSAC.2024.3459079

[20] F. Liu, L. Zheng, Y. Cui, C. Masouros, A. P. Petropulu, H. D. Griffiths, and Y. C. Eldar, "Seventy years of radar and communications: The road from separation to integration," *IEEE Signal Process. Mag.*, vol. 40, no. 5, pp. 106–121, 2023.
[21] X. Jing, F. Liu, C. Masouros, and Y. Zeng, "ISAC from the sky: UAV trajectory design for joint communication and target localization," *CoRR*, vol. abs/2207.02904, 2022.
[22] J. Wu, W. Yuan, and L. Bai, "On the interplay between sensing and communications for UAV trajectory design," *IEEE Internet Things J.*, vol. 10, no. 23, pp. 20 383–20 395, 2023.
[23] K. Meng, Q. Wu, J. Xu, W. Chen, Z. Feng, R. Schober, and A. L. Swindlehurst, "UAV-enabled integrated sensing and communication: Opportunities and challenges," *IEEE Wirel. Commun.*, vol. 31, no. 2, pp. 97–104, 2024.
[24] A. R. Chiriyath, B. Paul, G. M. Jacyna, and D. W. Bliss, "Inner bounds on performance of radar and communications co-existence," *IEEE Trans. Signal Process.*, vol. 64, no. 2, pp. 464–474, 2015.
[25] Y. Liu, S. Liu, X. Liu, Z. Liu, and T. S. Durrani, "Sensing fairness-based energy efficiency optimization for UAV enabled integrated sensing and communication," *IEEE Wirel. Commun. Lett.*, vol. 12, no. 10, pp. 1702–1706, 2023.
[26] O. Rezaei, M. M. Naghsh, S. M. Karbasi, and M. M. Nayebi, "Resource allocation for UAV-enabled integrated sensing and communication (ISAC) via multi-objective optimization," in *ICASSP 2023, Rhodes Island, Greece, June 4-10, 2023*.
[27] N. Huang, T. Wang, Y. Wu, Q. Wu, and T. Q. S. Quek, "Integrated sensing and communication assisted mobile edge computing: An energy-efficient design via intelligent reflecting surface," *IEEE Wirel. Commun. Lett.*, vol. 11, no. 10, pp. 2085–2089, 2022.
[28] Q. Qi, X. Chen, C. Zhong, and Z. Zhang, "Integrated sensing, computation and communication in B5G cellular Internet of Things," *IEEE Trans. Wirel. Commun.*, vol. 20, no. 1, pp. 332–344, 2021.
[29] N. Su, F. Liu, and C. Masouros, "Sensing-assisted eavesdropper estimation: An ISAC breakthrough in physical layer security," *IEEE Trans. Wirel. Commun.*, 2023.
[30] Y. Zeng, R. Zhang, and T. J. Lim, "Wireless communications with unmanned aerial vehicles: opportunities and challenges," *IEEE Commun. Mag.*, vol. 54, no. 5, pp. 36–42, 2016.
[31] X. Lin, V. Yajnanarayana, S. D. Muruganathan, S. Gao, H. Asplund, H. Maattanen, M. Bergström, S. Euler, and Y. E. Wang, "The sky is not the limit: LTE for unmanned aerial vehicles," *IEEE Commun. Mag.*, vol. 56, no. 4, pp. 204–210, 2018.
[32] H. Huang, S. Guo, W. Liang, K. Wang, and A. Y. Zomaya, "Green data-collection from GEO-distributed IoT networks through low-earth-orbit satellites," *IEEE Trans. Green Commun. Netw.*, vol. 3, no. 3, pp. 806–816, 2019.
[33] J. Choi and V. Chan, "Predicting and adapting satellite channels with weather-induced impairments," *IEEE Trans. Aerosp. Electron. Syst.*, vol. 38, no. 3, pp. 779–790, 2002.
[34] I. Del Portillo, B. G. Cameron, and E. F. Crawley, "A technical comparison of three low earth orbit satellite constellation systems to provide global broadband," *Acta astronautica*, vol. 159, pp. 123–135, 2019.
[35] T. Ma, H. Zhou, B. Qian, N. Cheng, X. Shen, X. Chen, and B. Bai, "UAV-LEO integrated backbone: A ubiquitous data collection approach for B5G internet of remote things networks," *IEEE J. Sel. Areas Commun.*, vol. 39, no. 11, pp. 3491–3505, 2021.
[36] Q. Qi, X. Chen, C. Zhong, and C. Y. Z. Zhang, "Deep learning-based design of uplink integrated sensing and communication," *IEEE Trans. Wirel. Commun.*, 2024.
[37] J. Zhang, J. Xu, W. Lu, N. Zhao, X. Wang, and D. Niyato, "Secure transmission for irs-aided uav-isac networks," *IEEE Trans. Wirel. Commun.*, 2024.
[38] Y. Wu, S. Tang, L. Zhang, L. Fan, X. Lei, and X. Chen, "Resilient machine learning-based semantic-aware MEC networks for sustainable next-G consumer electronics," *IEEE Trans. Consumer Electron.*, vol. 70, no. 1, pp. 2188–2199, 2024.
[39] R. Ding, F. Gao, and X. S. Shen, "3D UAV trajectory design and frequency band allocation for energy-efficient and fair communication: A deep reinforcement learning approach," *IEEE Trans. Wirel. Commun.*, vol. 19, no. 12, pp. 7796–7809, 2020.
[40] S. P. Boyd and L. Vandenberghe, *Convex optimization*. Cambridge university press, 2004.
[41] Q. Li, L. Shi, Z. Zhang, and G. Zheng, "Resource allocation in UAV-enabled wireless-powered MEC networks with hybrid passive and active communications," *IEEE Internet Things J.*, vol. 10, no. 3, pp. 2574–2588, 2023.
[42] Q. Qi, X. Chen, and C. Yuen, "Joint offloading selection and resource allocation for integrated localization and computing in edge-intelligent networks," *IEEE Trans. Vehic. Tech.*, pp. 1–15, 2024.
[43] G. Zhang, Q. Wu, M. Cui, and R. Zhang, "Securing UAV communications via joint trajectory and power control," *IEEE Trans. Wirel. Commun.*, vol. 18, no. 2, pp. 1376–1389, 2019.
[44] K. Meng, Q. Wu, S. Ma, W. Chen, K. Wang, and J. Li, "Throughput maximization for UAV-enabled integrated periodic sensing and communication," *IEEE Trans. Wirel. Commun.*, vol. 22, no. 1, pp. 671–687, 2023.

Xiangdong Zheng received the B.E. degree in 2022 and he is currently pursuing the master degree, with the School of Computer Science and Cyber Engineering, Guangzhou University, Guangzhou, China. His current research interests include Mobile Edge Computing, Wireless Power Transfer, Integrated Sensing and Communication, and Unmanned Aerial Vehicle Communication.

Yuxin Wu received the bachelor degree in Software Engineering from Northeastern university in 2018. He is currently pursuing the master degree with the school of Electronic and Information Engineering, Guangzhou University. His current research interests focus on mobile edge computing, integrated sensing and communication, and semantic communication.

Lisheng Fan received the bachelor and master degrees from Fudan University and Tsinghua University, China, in 2002 and 2005, respectively, both from the Department of Electronic Engineering. He received the Ph.D degree from the Department of Communications and Integrated Systems of Tokyo Institute of Technology, Japan, in 2008. He is now a Professor with GuangZhou University. His research interests span in the areas of wireless communications, artificial intelligence, intelligent communication, edge computing and system performance evaluation. Lisheng Fan has published many papers in international journals such as IEEE Transactions on Wireless Communications, IEEE Transactions on Communications, IEEE Transactions on Information Theory, as well as papers in conferences such as IEEE ICC, IEEE Globecom, and IEEE WCNC. He now serves as an Editor for IEEE Transactions on Vehicular Technology.

Authorized licensed use limited to: Aristotle University of Thessaloniki. Downloaded on September 23,2024 at 10:14:54 UTC from IEEE Xplore. Restrictions apply.
© 2024 IEEE. Personal use is permitted, but republication/redistribution requires IEEE permission. See https://www.ieee.org/publications/rights/index.html for more information.

This article has been accepted for publication in IEEE Journal on Selected Areas in Communications. This is the author's version which has not been fully edited and content may change prior to final publication. Citation information: DOI 10.1109/JSAC.2024.3459079

Xianfu Lei is currently a Professor with the School of Information Science and Technology at Southwest Jiaotong University (SWJTU). He received the Ph.D. degree from SWJTU in 2012. From 2012 to 2014, he worked as a Research Fellow in the Department of Electrical and Computer Engineering at Utah State University. His research interests are in the fields of communication theory and wireless networks. He has published nearly 150 technical papers in scientific journals and international conferences. He was a recipient of the IEEE Vehicular Technology Society Best Magazine Paper Award in 2023. He is serving as an executive editor for IEEE Communications Letters and an editor for IEEE Transactions on Communications, IEEE Communications Magazine, and IEEE Wireless Communications Letters. He was an area/senior editor for IEEE Communications Letters from 2019 to 2023. He also served as symposium/track and workshop chairs for major IEEE conferences.

Rose Qingyang Hu (Fellow, IEEE) received the B.S. degree from the University of Science and Technology of China, the M.S. degree from New York University, and the Ph.D. degree from the University of Kansas. Besides a decade academia experience, she has more than 10 years of R&D experience with Nortel, Blackberry, and Intel as a Technical Manager, a Senior Wireless System Architect, and a Senior Research Scientist, actively participating in industrial 4G technology development, standardization, system level simulation, and performance evaluation. She is a Professor with the Electrical and Computer Engineering Department and Associate Dean for research of College of Engineering at Utah State University. She also directs Communications Network Innovation Lab at Utah State University. Her current research interests include next-generation wireless system design, Internet of Things, Cyber Physical system, Mobile Edge Computing, V2X communications, AI/ML in wireless networks. She is currently serving on the editorial boards of the IEEE TRANSACTIONS ON WIRELESS COMMUNICATIONS, IEEE TRANSACTIONS ON VEHICULAR TECHNOLOGY, and IEEE WIRELESS COMMUNICATIONS. She also served as the TPC Co-Chair for the IEEE ICC 2018. She is an IEEE Communications Society Distinguished Lecturer Class 2015-2018, IEEE Vehicular Technology Society Distinguished Lecturer Class 2020-2022, and a recipient of prestigious Best Paper Awards from the IEEE GLOBECOM 2012, the IEEE ICC 2015, the IEEE VTC Spring and the IEEE ICC 2016. She is member of Phi Kappa Phi Honor Society.

George K. Karagiannidis (Fellow, IEEE) is currently Professor in the Electrical & Computer Engineering Dept. of Aristotle University of Thessaloniki, Greece and Head of Wireless Communications & Information Processing (WCIP) Group. He is also Faculty Fellow in the Cyber Security Systems and Applied AI Research Center, Lebanese American University. His research interests are in the areas of Wireless Communications Systems and Networks, Signal processing, Optical Wireless Communications, Wireless Power Transfer and Applications and Communications & Signal Processing for Biomedical Engineering. Dr. Karagiannidis was in the past Editor in several IEEE journals and from 2012 to 2015 he was the Editor-in Chief of IEEE Communications Letters. From September 2018 to June 2022 he served as Associate Editor-in Chief of IEEE Open Journal of Communications Society. Currently, he is the Editorin-Chief of IEEE Transactions on Communications. Recently, he received three prestigious awards: The 2021 IEEE ComSoc RCC Technical Recognition Award, the 2018 IEEE ComSoc SPCE Technical Recognition Award and the 2022 Humboldt Research Award from Alexander von Humboldt Foundation. Dr. Karagiannidis is one of the highly-cited authors across all areas of Electrical Engineering, recognized from Clarivate Analytics as Highly-Cited Researcher in the nine consecutive years 2015-2023.

Authorized licensed use limited to: Aristotle University of Thessaloniki. Downloaded on September 23,2024 at 10:14:54 UTC from IEEE Xplore. Restrictions apply.
© 2024 IEEE. Personal use is permitted, but republication/redistribution requires IEEE permission. See https://www.ieee.org/publications/rights/index.html for more information.